



HAL
open science

Enhancing micropollutant removal efficiency using sustainable activated charcoal

Taher Selmi, Solène Gentil, Vanessa Fierro, Alain Celzard

► **To cite this version:**

Taher Selmi, Solène Gentil, Vanessa Fierro, Alain Celzard. Enhancing micropollutant removal efficiency using sustainable activated charcoal. *Journal of Environmental Chemical Engineering*, 2024, 12 (6), pp.114855. 10.1016/j.jece.2024.114855 . hal-04961117

HAL Id: hal-04961117

<https://hal.univ-lorraine.fr/hal-04961117v1>

Submitted on 21 Feb 2025

HAL is a multi-disciplinary open access archive for the deposit and dissemination of scientific research documents, whether they are published or not. The documents may come from teaching and research institutions in France or abroad, or from public or private research centers.

L'archive ouverte pluridisciplinaire **HAL**, est destinée au dépôt et à la diffusion de documents scientifiques de niveau recherche, publiés ou non, émanant des établissements d'enseignement et de recherche français ou étrangers, des laboratoires publics ou privés.

1 Enhancing micropollutant removal efficiency using
2 sustainable activated charcoal

3
4 Taher Selmi^{1,2,*}, Solène Gentil², Vanessa Fierro¹, Alain Celzard^{1,3,*}

5
6
7 ¹ Université de Lorraine, CNRS IJL, F-88000 Epinal, France

8 ² Groupe BORDET, Froidvent, F-21290 Leuglay, France

9 ³ Institut Universitaire de France (IUF), F-75231 Paris, France

10

11

* Corresponding authors. E-mails: taher.selmi@univ-lorraine.fr; alain.celzard@univ-lorraine.fr

1 **Abstract**

2 This study aims to develop a sustainable and low-cost activated carbon (AC) from wood
3 charcoal to improve the removal of persistent micropollutants, such as pesticides, drug
4 residues, and per- and polyfluoroalkyl substances (PFAS), from drinking water. The AC was
5 produced through physical activation using steam in a rotary furnace, with activation
6 temperatures ranging from 850 to 900 °C and times varying from 1 to 2.5 hours. The textural
7 properties, adsorption kinetics, equilibrium behaviour, and potential adsorption mechanisms
8 of the AC were thoroughly investigated. N₂ adsorption isotherms revealed a transition from
9 microporous to mesoporous structures as both activation time and temperature increased,
10 resulting in BET areas between 600 and 1380 m²/g. Among the produced ACs, one was
11 selected for its outstanding performance in removing micropollutants, demonstrating rapid
12 adsorption kinetics even at low AC doses and high pollutant concentrations. The adsorption
13 kinetics were well described by a model suggesting fractal adsorption behaviour, while
14 isotherms indicated multilayer adsorption for certain micropollutants, with additional models
15 providing insights into molecular aggregation and anchoring geometry. This AC exhibited
16 unprecedented efficiency in removing micropollutants, particularly PFAS, reaching 1977, 670
17 and 3135 mg/g for perfluorooctanoic acid, perfluorooctanesulfonic and perfluorohexanoic
18 acid, respectively, and outperformed commercial ACs due to its optimized mesoporous
19 structure.

20

21

22 **Keywords:** Persistent micropollutants removal; PFAS; Drugs; Pesticides; Sustainable
23 activated carbon.

24

1 **1. Introduction**

2 The use of organic chemicals in municipal, industrial, and agricultural activities has
3 surged, leading to the proliferation of persistent organic pollutants (POPs) as defined by the
4 Stockholm Convention [1]. These include drug residues, pesticides and their metabolites, as
5 well as so-called "eternal" micropollutants like PFAS (per- and polyfluoroalkyl substances).
6 PFAS have recently sparked significant controversy and are now the focus of European
7 legislation aimed at banning them. In addition, the repeated discovery of atrazine (ATZ), its
8 metabolites (desethyl atrazine (DEA)) and, several other pesticides in tap water is a cause
9 for concern, despite bans for years [2]. Similarly, PFAS molecules are still found in water
10 even after production and use bans imposed in 2009 (perfluorooctanesulfonic acid: PFOS),
11 2020 (perfluorooctanoic acid: PFOA) and 2022 (perfluorohexanoic acid: PFHxA) [3-7].
12 Drug residues such as paracetamol (PARA), carbamazepine (CBZ), ciprofloxacin (CIP), and
13 17 β -estradiol (17 BE) are increasingly detected in water at concentrations up to 100 $\mu\text{g/L}$
14 [6,8-12]. Many of these chemicals and their metabolites are toxic or carcinogenic to humans
15 [13-25]. The International Agency for Research on Cancer has thus classified PFOS and
16 PFOA as "possibly carcinogenic" and "carcinogenic to humans", respectively [26].

17 The presence of these chemicals in water has led to advanced treatment processes aimed to
18 reduce their concentration to meet European Water Directive [27]. However, these processes
19 must be evaluated and optimized for technical and economic feasibility in drinking water
20 production. Activated carbon (AC) is widely used for its effectiveness in removing organic
21 micropollutants, thanks to its high adsorption capacity and ability to regenerate [28-34]. These
22 advantages make AC more sustainable and cost-effective than other methods, such as
23 exchange resins, membrane filtration (microfiltration, ultrafiltration, nanofiltration and reverse
24 osmosis), oxidation (advanced oxidation, ultraviolet irradiation and electro dialysis). [34-39].

1 To guarantee effective water purification, selecting the appropriate AC requires careful
2 consideration of several factors. Our recent study [23] identified that the optimal AC should
3 possess a high BET area ($> 1000 \text{ m}^2/\text{g}$), 65-80% microporosity and 20-35% mesoporosity. Yet,
4 suitable surface functional groups are also required: nitriles, pyridines and amides for PFAS
5 removal; carbonyl, phenolic, lactone, quinone and amine groups for drug adsorption; basic
6 oxygen (*e.g.* pyrones) and amine groups for DEA and ATZ removal; and hydrophobic (*e.g.*
7 alkyl) and electrophilic (*e.g.* carboxylic acid, phenol groups.) for metolachlor ethanesulfonic
8 acid (MET ESA) removal.

9 With evolving regulations requiring lower micropollutant concentrations and the
10 extensive use of mineral or imported plant-based ACs, research into eco-friendly AC
11 production is essential. Recent studies have explored biomass-based ACs from materials
12 such as pecan nutshells, oil palm shells, English nutshells, apple waste, artichoke leaves,
13 pomegranate peels. [31,40-44]. Sustainable activated carbons can also be produced from
14 waste products such as chitosan flakes [45], oil palm ash [46], rattan hydrochar [47], karanj
15 fruit hulls [48], chitin [49], chitosan/sepiolite composites [50], zeolite/chitosan composites
16 from oil palm ash [51,52] for the removal of pollutant dyes (methylene blue, reactive orange
17 16 and acid blue 29) and antibiotics (tetracycline and cephalixin). Optimizing AC production
18 and adsorption mechanisms can enhance selectivity for targeted micropollutants. AC
19 selectivity can also be improved by functionalizing its surface, *i.e.*, creating surface
20 functions that enable it to bind these micropollutants more effectively [53-59]. For instance,
21 the addition of a cationic polymer (poly diallyldimethylammonium chloride) to commercial
22 AC Filtrasorb 400 increased PFOS adsorption capacities from 165 mg/g to 270 mg/g [53].

23 This study aims to develop a sustainable and cost-effective activated carbon (AC) from
24 hardwood charcoal industrially produced by Groupe Bordet using physical activation to
25 improve the removal of a wide range of micropollutants from water, including pesticides

1 (ATZ, DEA and MET ESA), pharmaceuticals (PARA, CBZ, CIP and 17 BE) and PFAS
2 (PFOS, PFOA and PFHxA), unlike other activated carbons. These molecules were selected
3 based on our study published in August 2024 [23], which demonstrates their presence in tap
4 water. The study examines the AC's physicochemical properties, adsorption kinetics,
5 equilibrium behavior and potential adsorption mechanisms using classical and stochastic
6 fractal models based on statistical physics formalism. Comparative analyses with commercial
7 ACs provided benchmarks to evaluate its performance and competitiveness.

8 **2. Material and methods**

9 **2.1. Activated carbon precursor and chemicals used**

10 The activated carbon (AC) used in this study was derived from Groupe Bordet's vegetable
11 carbon, produced by slow and continuous wood pyrolysis. The process involves the pyrolysis
12 of hardwood at 600 °C for 12 h in a closed circuit, in which tars and gases are recycled to a
13 burner ensuring the energy self-sufficiency of the entire system. Complete by-product
14 extraction and continuous production guarantee the high purity of Groupe Bordet's vegetable
15 charcoal.

16 Micropollutants used for adsorption testing included pesticides (ATZ, DEA and MET
17 ESA), pharmaceuticals (PARA, CBZ, CIP and 17 BE), and PFAS (PFOS, PFOA and
18 PFHxA). Except for PFHxA, which was purchased from Sigma-Aldrich, all other molecules
19 were purchased from VWR with a purity of over 96%. The physicochemical characteristics of
20 these micropollutants and their effects on human health have been summarized elsewhere
21 [23].

22 **2.2. Activated carbon synthesis**

23 Physical activation with steam was carried out using a horizontal rotary tube furnace
24 (CARBOLITE TSO 11/800). For that purpose, 200 g of Groupe Bordet's vegetable charcoal
25 with a particle size of 3-8 mm was transferred to a quartz reactor placed in the furnace, then

1 purged with high-purity nitrogen (99.99%) at a flow rate of 300 mL/min for 1 hour at room
2 temperature. The activation occurred in two steps: (a) heating at 5 °C/min from room
3 temperature to 850 or 900 °C; and (b) maintaining the temperature and injecting water at a
4 rate of 6 mL/min for different activation times (0.5, 1, 1.5, 2 or 2.5 hours). Throughout the
5 activation process, the vegetable charcoal was stirred in the quartz reactor by rotation at 6
6 rpm. The furnace was then cooled under a nitrogen flow of 300 mL/min. The ACs were
7 labeled ACT-t, where "T" stands for activation temperature (°C) and "t" for activation time
8 (h). For instance, AC850°C-2h represents the charcoal activated at 850 °C for 2h.

9 **2.3. Activated carbon characterization**

10 The ACs produced were then characterized to determine their physicochemical
11 characteristics. Textural properties were determined by performing nitrogen adsorption-
12 desorption isotherms at -196 °C using an ASAP 2020 Micromeritics automatic device. The
13 BET (Brunauer-Emmett-Teller) model was applied to the nitrogen adsorption isotherms to
14 calculate the BET area, A_{BET} [60]. Pore size distribution (PSD, for micropores and mesopores)
15 was determined by application of the non-local density functional theory (NLDFT) using
16 SAIEUS® software. In addition, total pore volume (V_{tot}), micropore volume (V_{mic}), and
17 mesopore volume (V_{mes}) were calculated by integrating the PSD over the entire pore size
18 range, with mesopore volume deduced from the difference between V_{tot} and V_{mic} [61-64].

19 The pH drift method was applied to determine the pH of the point of zero-charge (pH_{PZC}),
20 which indicates the pH at which the surface of an activated carbon is neutral. This method
21 involves the preparation of 0.01 M NaCl solutions, adjusted to different pH values, followed
22 by measurement of the final pH after 48 hours of stirring using a Metrohm pH meter. The
23 pH_{PZC} was identified as the point of intersection of the initial versus final pH curves [65].

24 The amount and nature of surface functional groups were also determined by
25 potentiometric titration using an automatic titrator (905 Titrand, Metrohm controlled with

1 tiamo® software V2.2). Details of the method are described elsewhere [66]. Briefly, 0.1 g of
2 AC was placed in 50 mL of 0.01 M NaNO₃ solution. 1 mL of 1 M HCl was then added to the
3 solution. The mixture was stirred for 24 h and titrated with 0.1 M NaOH under N₂ flow at
4 saturation. The number of proton-binding functional groups was evaluated, allowing the total
5 surface charge σ (mmol/g) to be calculated. From this information, the number of groups with
6 pKa values in selected ranges was used to determine the type and amount of surface functions
7 [67,68]. The pKa distribution was determined using the SAIEUS® numerical calculation.

8 AC elemental composition (C, H, O, N and S) was determined using a vario EL Cube
9 (Elementar, Germany) elemental analyzer. Ash, moisture, fixed carbon and volatile matter
10 contents were determined by thermogravimetric analysis (STA 449F3 Jupiter microbalance,
11 Netzsch) in an inert atmosphere using argon gas. The moisture content was calculated based
12 on mass loss at 105 °C after a heating at 4 °C/min from room temperature and a 1 h isotherm.
13 The temperature was then increased at 10 °C/min to 900 °C, and volatile matter was
14 calculated by mass loss after a 30-min isotherm. The ash content was assessed by air injection
15 at 900 °C for 30 minutes.

16 **2.4. Adsorption tests**

17 *2.4.1. Experimental details*

18 Batch experiments were conducted to study the adsorption kinetics and isotherms of the
19 aforementioned micropollutants on activated carbon. To assess adsorption kinetics, solutions
20 containing micropollutants at defined concentrations were stirred in the presence of a known
21 dose (AC mass / volume of micropollutant solution). At defined time intervals, samples were
22 collected for analysis using an appropriate detection technique. The initial concentrations, AC
23 doses, and analytical methods used are summarized in Table 1. The HPLC, UPLC/MS/MS
24 and UV-Vis spectroscopy methods applied are detailed in Section VI of the Supplementary

1 Information (SI). A diagram of the experimental set-up in Figure SI 6 summarizes the steps
 2 followed.

3 Adsorption isotherms were determined by mixing a mass of AC in a volume of solution
 4 containing micropollutants at different initial concentrations (see Table 1). After 24 hours,
 5 residual concentrations were measured using appropriate analytical techniques (see Table 1).
 6 The amount of micropollutants adsorbed at time t , q_t (mg/g), and removal, R (%), were
 7 calculated as follows:

$$8 \quad q_t = \frac{C_i - C_t}{m} \times V \quad \text{Equation 1}$$

$$9 \quad R(\%) = \frac{C_i - C_f}{C_i} \times 100 \quad \text{Equation 2}$$

10 where C_i , C_f and C_t (mg/L) are initial, final and the concentrations at time t , respectively, V
 11 (L) is the volume of the micropollutant solution, and m (g) is the mass of AC.

12 A comparison of atrazine (ATZ) adsorption on the synthesized AC at different initial
 13 concentrations (1-10 mg/L) and for different contact times (1-24 h) was carried out using a
 14 mineral AC produced by Calgon Carbon from bituminous coal, called Filtrasorb 300 (F300),
 15 and a coconut-based activated carbon used in Brita filters, here referred to as Brita AC [69].

16 Table 1: Different parameters used for adsorption tests.

Pollutant	Kinetic parameters		Isotherm parameters		Analytical techniques
	C_i (mg/L)	Dose (g AC/L)	C_i (mg/L)	Dose (g AC/L)	
ATZ	9.93	1	1-30	0.2	UV-Vis spectrophotometer, $\lambda = 222$ nm
DEA	0.55-31.21	0.2	0.5-30	0.2	UV-Vis spectrophotometer, $\lambda = 214$ nm
MET ESA	6.59	0.2	1-100	0.2	UPLC/MS/MS
PARA	96.87	0.2	1-500	0.2	UV-Vis spectrophotometer, $\lambda = 243$ nm
CBZ	1.01-15.81	0.2	1-16	0.2	UV-Vis spectrophotometer, $\lambda = 285$ nm

CIP	1.28-113.68	0.2	1-100	0.2	UV-Vis spectrophotometer, $\lambda = 272$ nm
17 BE	2.04	0.05	0.05-3	0.05	HPLC
PFOS	4.80	0.2	5-400	0.2	UPLC/MS/MS
PFOA	5.10	1	5-500	0.2	UPLC/MS/MS
PFHxA	15.80	0.2	10-1000	0.2	UPLC/MS/MS

1

2 2.4.2. Kinetic modeling

3 Experimental kinetic data were fitted by classical kinetics models such as the Lagergren
4 model [70] (pseudo-first order (PFO) model) and the Ho and Mckay model [71] (pseudo-
5 second order (PSO) model). These two models are described by the following equations,
6 respectively:

$$7 \quad q_t = q_{e,1} (1 - \exp(-k_1 t)) \quad \text{Equation 3}$$

$$8 \quad q_t = \frac{q_{e,2}^2 k_2 t}{1 + q_{e,2} k_2 t} \quad \text{Equation 4}$$

9 where k_1 (1/min) and k_2 (g/mg/min) represent the rate constants, and $q_{e,1}$ (mg/g) and $q_{e,2}$
10 (mg/g) represent the equilibrium adsorption quantities of the PFO and PSO models,
11 respectively.

12 A fractal model based on statistical physics, known as Brouers-Sotolongo fractal (BSf)
13 model [72] model was also applied. This model is described as follows:

$$14 \quad q_{n,\alpha}(t) = q_{e,BSf} \left[1 - \left(1 + (n-1) \left(\frac{t}{\tau_{n,\alpha}} \right)^\alpha \right)^{\frac{-1}{(n-1)}} \right] \quad \text{Equation 5}$$

15 where $q_{e,BSf}$ (mg/g), n , $\tau_{n,\alpha}$ (min) and α represent respectively the equilibrium adsorption
16 amount (mg/g), the non-integer reaction order, the estimated characteristic time to reach
17 equilibrium (min), and the fractional time of adsorption reaction giving information on
18 surface fractal nature and heterogeneity. Further details on the physical significance of these
19 parameters are available elsewhere [73].

1 2.4.3. Isotherm modeling

2 Micropollutant adsorption data obtained at equilibrium were studied using the classical
3 isotherm models of Freundlich [74] and Langmuir [75]:

$$4 \quad q_{eF} = K_F C_e^{1/n_F} \quad \text{Equation 6}$$

$$5 \quad q_{eL} = \frac{q_{e \max,L} K_L C_e}{1 + K_L C_e} \quad \text{Equation 7}$$

6 where n_F and K_F (mg/g)(L/mg)^{1/n_F} represent the Freundlich model constants, indicating
7 adsorption affinity and adsorption capacity, respectively. K_L (L/mg) and $q_{e \max,L}$ (mg/g) are the
8 Langmuir constant and the maximum adsorption capacity estimated by the Langmuir model,
9 respectively.

10 The stochastic model known as General Brouers-Sotolongo (GBS) [76,77] model was also
11 applied to describe the micropollutant isotherm data. It is described by the following equation:

$$12 \quad q_{e \text{ GBS}} = q_{e \max, \text{GBS}} \left(1 - \left[1 + c \left(\frac{C_e}{b} \right)^a \right]^{-1/c} \right) \quad \text{Equation 8}$$

13 where $q_{e \max, \text{GBS}}$ is the maximum adsorption capacity estimated by GBS model, a is the
14 measure of the surface energy heterogeneity, b is related to the equilibrium concentration and
15 can therefore be used to predict adsorbed amount at equilibrium, and c is correlated to the
16 fractal distribution of pores or the aggregation and clustering of adsorbent particles. The
17 physical meaning of these parameters is detailed elsewhere [73], and the rationale for
18 applying the BSf and GBS models to adsorption kinetics and isotherms, respectively, is
19 provided in section VII of the Supplementary Information (SI).

20 Models derived from statistical physics have also been applied to study the micropollutant
21 adsorption isotherms. Here, we have chosen a model capable of describing monolayer
22 adsorption with two sites of different adsorption energies (MLM2E) and a model capable of
23 describing bilayer adsorption with two sites of different adsorption energy (DLM2E) [78,79].

24 These models have been described by the following equations, respectively:

$$q_{e,MLM2E} = \frac{n_1 D_1}{1 + \left(\frac{C_1}{C_e}\right)^{n_1}} + \frac{n_2 D_2}{1 + \left(\frac{C_2}{C_e}\right)^{n_2}} \quad \text{Equation 9}$$

with n_i is the number of molecules adsorbed per adsorption site and D_i (mg/g) is the density of these active adsorption sites. C_1 and C_2 (mg/L) are the half-saturation concentrations for the first and second adsorption sites, respectively. $n_1 D_1 = q_{e\ max,1}$ and $n_2 D_2 = q_{e\ max,2}$ are the maximum adsorption capacity of the first and second adsorption sites, respectively. The total maximum adsorption capacity predicted by MLM2E, $q_{e\ max,MLM2E}$, is equal to $q_{e\ max,1} + q_{e\ max,2}$:

$$q_{e,DLM2E} = nD \frac{\left(\frac{C_e}{C_{0,1}}\right)^n + 2\left(\frac{C_e}{C_{0,2}}\right)^{2n}}{1 + \left(\frac{C_e}{C_{0,1}}\right)^n + \left(\frac{C_e}{C_{0,2}}\right)^{2n}} \quad \text{Equation 10}$$

where n and D have the same meaning as above, and C_{01} and C_{02} are the half-saturation concentrations for the first and second layers, respectively. $2nD = q_{e\ max,DLM2E}$, where 2 is the number of layers, is the maximum adsorption capacity of the two adsorption layers estimated by the DLM2E model. Further details on the physical significance of the parameters of the MLM2E and DLM2E models can be found elsewhere [78-82].

The Levenberg-Marquardt iteration algorithm provided with OriginPro® 2021 software was used to determine the parameters of the kinetic and isotherm models. The higher the determination coefficient (R^2) and the lower the fit error (χ^2), the better the model describes the data. The parameters R^2 and χ^2 were calculated as detailed elsewhere [65].

3. Results and discussion

3.1. Properties of the synthesized activated charcoals

3.1.1. Textural properties

Vegetable charcoals activated at different times and temperatures were subjected to characterization in order to identify their textural properties. Figure 1 and Figure SI 1 show the N_2 adsorption-desorption isotherms at $-196\ ^\circ\text{C}$ for charcoals activated at $850\ ^\circ\text{C}$ and 900

1 °C, respectively, at various activation times. To clarify the discussion, the textural properties
2 obtained after activation at 900° C are reported in Table SI I, but the same conclusions can be
3 drawn.

4 The longer the activation time, the greater the volume of nitrogen adsorbed. The nitrogen
5 isotherms show a significant adsorbed amount at low pressure, suggesting a well-developed
6 microporosity. At a certain relative pressure ($P/P^\circ = 0.01$), a plateau begins to form, with a
7 close knee and very narrow hysteresis loops for non-activated charcoal or charcoal activated
8 for 0.5 h. These isotherms are classified as type I(b), according to the IUPAC classification
9 [83], indicating a purely microporous AC with a relatively small external surface area and
10 narrow micropores ($< \sim 1$ nm) [83].

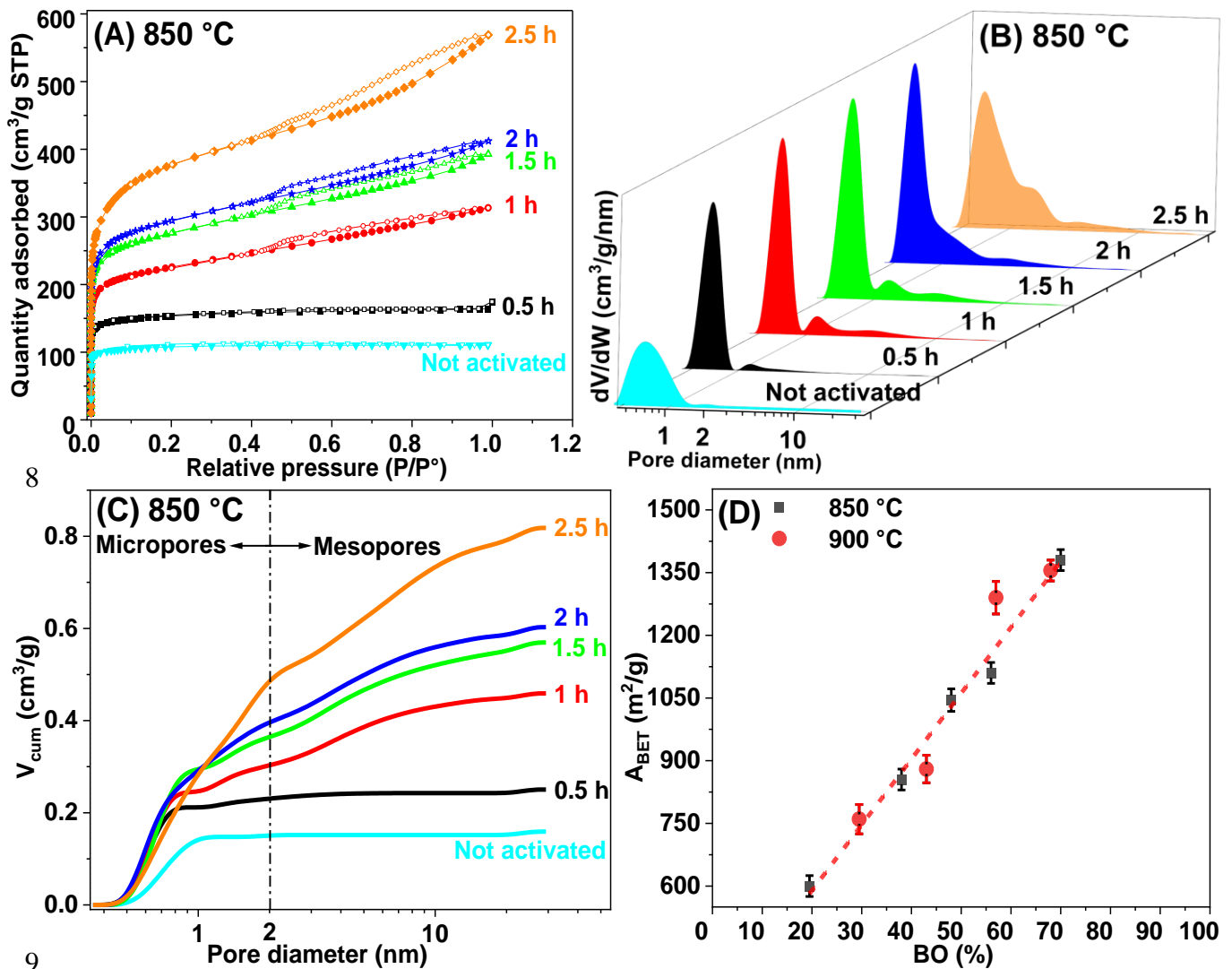
11 Beyond 0.5 h of activation, the hysteresis at $P/P^\circ = 0.4$ and the knee of the isotherm start to
12 widen, accompanied by an upward curvature that increases with activation time. This
13 corresponds to type II isotherms according to the IUPAC classification [83]. This behavior is
14 attributed to the progressive enlargement of micropores and the formation of mesopores.
15 These results are confirmed by analysis of the pore size distribution (PSD) and cumulative
16 volumes, as shown in Figure 1B and 1C, respectively, and in Figure SI 1.

17 Vegetable charcoal carbon precursor (*i.e.*, before activation) and AC-0.5h are
18 predominantly microporous, with an average pore size of 0.6 nm. The peak of the micropore
19 size distribution (dv/dw) grows until 2 h of activation at 850 °C (and 1.5 h of activation at 900
20 °C), indicating the formation of new micropores as a function of activation time. Beyond
21 these times, the peak begins to decrease and the distribution peaks widen towards the
22 mesopore region, signaling the progressive transformation of an increasing portion of
23 micropores into mesopores and macropores. For activation times of less than 2 h at 850 °C
24 (and 1.5 h at 900 °C), the creation of micropores predominates over that of mesopores.
25 Beyond that point, the enlargement of micropores into mesopores takes precedence over the

1 creation of new micropores. All these observations are clearly reflected in the variation of
2 cumulative pore volumes as a function of activation time (Figure 1C and Figure SI 1). For
3 pore diameters below 1 nm, the cumulative volumes increase with activation time up to 2 h at
4 850 °C (and 1.5 h at 900 °C), after which they progressively decrease. For pore diameters
5 greater than 2 nm, the cumulative volumes increase with activation time (with the exception
6 of 2 h activation at 900 °C), confirming mesopore formation. For pore diameters larger than 4
7 nm, the cumulative volumes begin to become lower after 1.5 h of activation at 900 °C (see
8 Figure SI 1C), confirming the transformation of pores into large mesopores and macropores.
9 Investigating the effect of several AC synthesis conditions, Kim *et al.* [84] found the same
10 trend. After increasing the activation temperature from 800 to 900 °C, an optimal activation
11 time (50 min) was found to obtain the highest values of V_{tot} (0.66 cm³/g), V_{mic} (0.57 cm³/g),
12 V_{mes} (0.09 cm³/g) and A_{BET} (1403 m²/g).

13 Figure 1D shows the variation of A_{BET} as a function of mass loss after activation, here
14 referred to as burn-off (BO, %). The variation of V_{tot} , V_{mic} , and V_{mes} as a function of BO is
15 illustrated in Figure SI 2 and Table SI 1. For the same activation time, the BO at 900 °C is
16 higher than at 850 °C, indicating faster activation at higher temperature. High BET areas of
17 1380 and 1355 m²/g are achieved at 850 °C and 900 °C after 2.5 and 2 h of activation,
18 respectively. The BET area increases linearly with BO at 850 °C. However, after 2 h of
19 activation at 900 °C, A_{BET} increases only slightly before stabilizing (or even decreasing after
20 this point), which may be due to the onset of material degradation and/or the transformation
21 of micropores and mesopores into macropores, undetectable by nitrogen adsorption
22 experiments [85]. Similar results were found by Hayrera *et al.* [86] when they studied the
23 effect of activation conditions (temperature: 600, 800 or 900 °C, and time: 1, 2 or 3 h) on AC
24 production. These authors found that increasing activation time and temperature no longer
25 significantly increased A_{BET} beyond 2 h and 900 °C.

1 Finally, the decrease in V_{tot} and V_{mes} after 2 h of activation at 900 °C confirms the
 2 transformation of micropores, formed at short activation times, into mesopores and
 3 macropores during long activation times, showing that under specific conditions (long
 4 activation times and high activation temperatures) activation can become excessive,
 5 necessitating an adjustment of parameters to meet specific objectives. These conclusions have
 6 also been drawn in several publications [87] when investigating the effect of synthesis
 7 conditions on the porous texture of AC.



10 Figure 1: (A) N₂ adsorption-desorption isotherms; (B) pore size distributions (PSD); and (C)
 11 cumulative pore volumes of charcoal activated at 850 °C and different activation
 12 times. (D) Variation of BET area as function of burn-off after activation at 850 and
 13 900 °C.

1 Based on the results of the textural characterizations, we selected one AC in order to
2 determine its properties and carry out micropollutant adsorption tests. The choice of this AC
3 was guided by the need to meet the physicochemical characteristics required for efficient
4 adsorption of the micropollutant under study, as detailed in a previous work [23]. In brief, the
5 targeted physicochemical properties are as follows: $A_{\text{BET}} > 1000 \text{ m}^2/\text{g}$, mesopore fraction
6 between 25 and 35 % of total pore volume, and pH_{PZC} above solution pH. We also considered
7 economic factors, choosing an AC that met these criteria while offering the lowest possible
8 activation temperature, activation time and mass loss. Given these conditions, AC850°C-2h
9 was selected for the next steps in this study.

10 In our adsorption tests, we compared the adsorption of ATZ with two commercial activated
11 carbons: F300 and Brita AC. To better interpret the observed results, we carried out textural
12 characterizations of these three ACs, allowing us to identify their impact on ATZ removal
13 efficiency. The data obtained are summarized in Figure 2 and Table SI 5. Figure 2A shows
14 that F300 exhibits a type Ib isotherm, characteristic of a microporous adsorbent with slightly
15 larger micropores than those of the type Ia isotherm observed for Brita AC, which
16 corresponds to a purely microporous activated carbon. Table SI 5 shows that Brita AC has the
17 lowest fraction of mesopores (9%), compared with AC850°C-2h (33.5%) and F300 (26%).
18 This is reflected in the A_{BET} , which is $1025 \text{ m}^2/\text{g}$ for Brita AC, comparable to that of
19 AC850°C-2h ($1110 \text{ m}^2/\text{g}$), while F300 has a slightly lower A_{BET} ($885 \text{ m}^2/\text{g}$). As clearly shown
20 in Figure 2B, AC850°C-2h exhibits higher mesopore and micropore volumes than the two
21 selected commercial activated carbons. Its mesopore volume is particularly noteworthy, at
22 $0.21 \text{ cm}^3/\text{g}$, compared to $0.04 \text{ cm}^3/\text{g}$ for Brita AC and $0.11 \text{ cm}^3/\text{g}$ for F300.

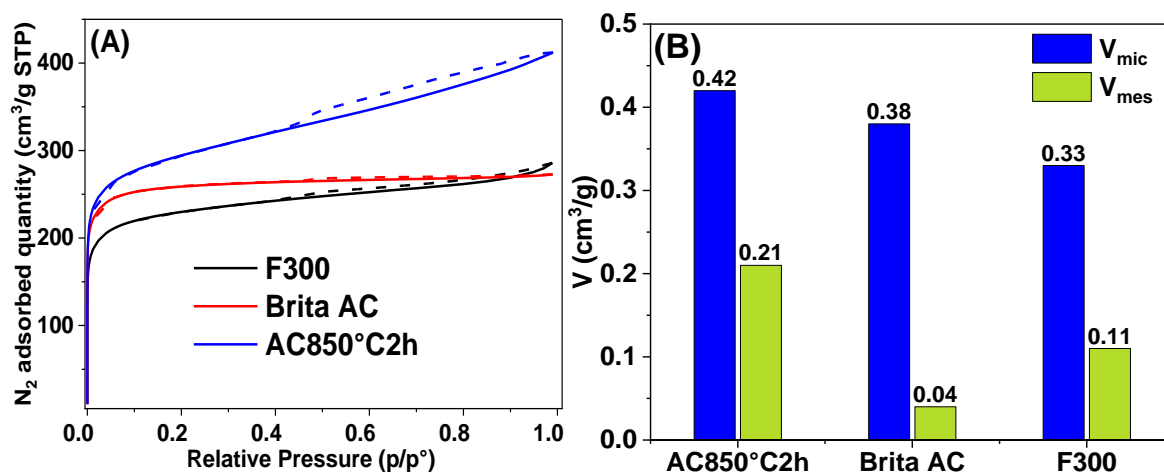


Figure 2: (A) N₂ adsorption-desorption isotherm and (B) micro and mesopore volumes for AC850°C-2h compared with Brita AC and F300 commercial activated carbons.

3.1.2. Chemical composition

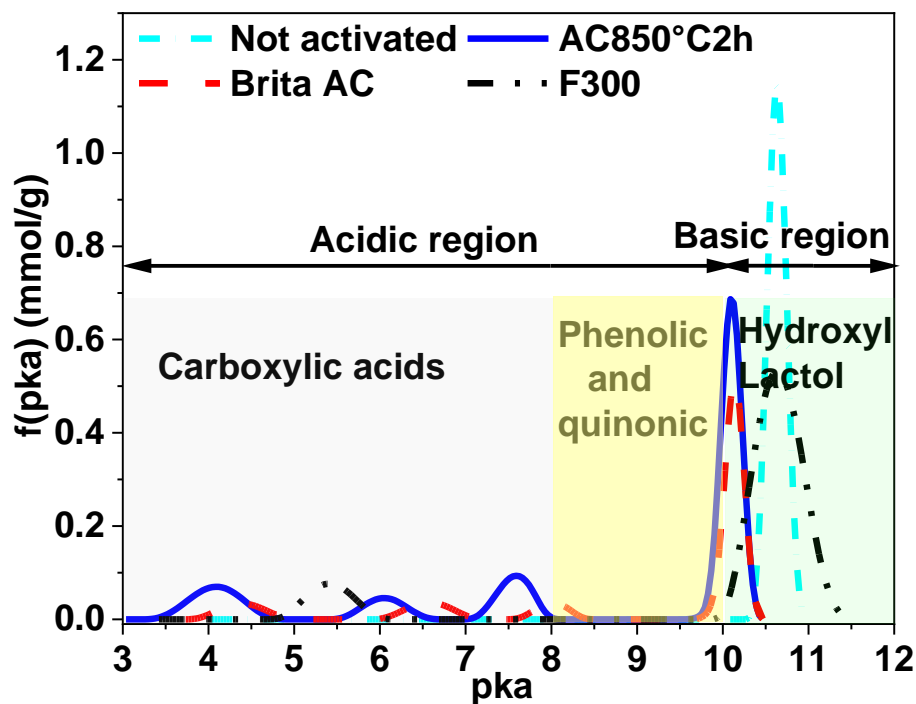
As AC850°C-2h was chosen for micropollutant adsorption tests, further characterization of chemical composition, pH_{PZC} and functional groups was carried out to better explain and discuss its micropollutant adsorption performance. The elemental composition results were compared with those of the vegetable charcoal precursor. The results for the functional groups were compared with those of Brita AC and F300 used in the benchmarking studies in Section 3.2.5.

The charcoal from Groupe Bordet stands out for its exceptional purity, with a carbon content close to 90%. Its precise composition is 89.13 wt.% C, 8.09 wt.% O, 2.55 wt.% H and 0.23 wt.% N. It has a moisture content of 2.24 wt.%, a volatile matter content of 8.48 wt.%, a fixed carbon content of 89.26 wt.%, and an ash content of 1.56 wt.%. This composition reflects high quality and outstanding purity, making Groupe Bordet's charcoal particularly suitable for applications such as AC production for drinking water treatment.

In comparison, AC850°C-2h charcoal exhibits distinctive characteristics. According to elemental analysis, it contains 91.83 wt.% C, 4.17 wt.% O, 0.74 wt.% H and 0.18 wt.% N.

1 Thermogravimetric analysis (see Figure SI 3) reveals a moisture content of 1.08 wt.% and
2 volatile matter content of 4.04 wt.%, significantly lower than those observed for Groupe
3 Bordet's charcoal, as a direct result of the high-temperature activation stage. Activation
4 considerably reduces moisture content and volatile matter by over 50%. AC850°C-2h also has
5 a higher fixed carbon content of 94.11 wt.% and a slightly higher ash content of 1.85 wt.%,
6 due to steam activation.

7 Figure 3 illustrates the distribution of surface functional groups as a function of their
8 acidity constant (pKa) for the non-activated charcoal, AC850°C-2h, as well as for the
9 commercial activated carbons Brita AC and F300. The corresponding data, as well as the
10 pH_{PZC} of AC850°C-2h and F300, are given in Table SI 2. Figure 3 shows that AC850°C-2h
11 and Brita AC have four peaks of surface functions, indicating their variety. In contrast, F300
12 shows only two peaks, and the non-activated charcoal only one. This highlights the
13 importance of the nature of the raw material to be activated, since AC850°C-2h and Brita AC,
14 vegetable charcoals derived from wood and coconut, respectively, show greater functional
15 diversity than F300, an activated bituminous coal. Selmi *et al.* (2018) [73] observed a similar
16 trend by analyzing the surface functional groups of two activated carbons of plant origin
17 (Acticarbone and Cecalite) and two activated carbons of mineral origin (F200 and F300).
18 Their findings indicate that plant-based ACs exhibit greater diversity and abundance of
19 surface functional groups than mineral ACs. Steam activation of Groupe Bordet's vegetable
20 charcoal led to the emergence of surface functions within a pKa range from 3 to 8, thus
21 considerably enriching the material's surface chemistry.



1
 2 Figure 3: Distribution of surface functional groups as a function of pKa for the three ACs
 3 under study.

4 Traditionally, surface functional groups located in the pKa region of 3 – 8 are
 5 predominantly carboxylic acids, while those in the pKa region of 8 – 10 are usually phenolic
 6 and quinonic functions [66,73]. The amount of surface functions in the pKa range 3 - 10
 7 represents the total of acidic functions, while the pKa region 10 - 12 corresponds to the total
 8 of basic surface functions. The pKa distributions reveal a predominance of basic functional
 9 groups, such as hydroxyl or lactol groups, on ACs. This basicity is confirmed by the high
 10 pH_{PZC} values observed for AC850°C-2h and F300, which are 9.31 and 9.03, respectively.
 11 These values indicate that the surface of these carbons is predominantly basic, enhancing their
 12 ability to adsorb acidic compounds such as PFAS.

13
 14 **3.2. Micropollutant adsorption**

15 *3.2.1. General considerations*

16 The micropollutant adsorption kinetics, illustrated in Figure 4, can be categorized into two
 17 distinct phases. In the first phase, kinetics increase rapidly over short time intervals, mainly

1 due to the rapid diffusion of molecules toward the available active sites, as well as the
2 abundance of free molecules in the solution. Subsequently, these kinetics gradually slow
3 down until equilibrium is reached, more or less pronounced depending on the micropollutants
4 under consideration. This slowdown is attributed to a slower diffusion of molecules towards
5 the active sites, which become progressively less accessible, and to a reduction in the number
6 of free molecules in solution [65].

7 As the initial concentration of free molecules in the solution increases, the diffusion rate of
8 these molecules toward the AC pores also increases, leading to a greater quantity adsorbed up
9 to a certain point. Beyond this initial concentration threshold, diffusion becomes progressively
10 slower as the free molecules present in the solution tend to diffuse simultaneously, clogging
11 the AC pores and slowing down the adsorption process. Consequently, the time required to
12 reach equilibrium increases with the initial concentration. The behavior of DEA, CBZ, and
13 CIP micropollutants adsorption kinetics (see Figure SI 4) clearly confirms this phenomenon:
14 as the initial concentration increases, the adsorption kinetic curves at the first instants have a
15 steeper slope, but this cannot increase indefinitely, so that they end up merging at short times.
16 The same trend was observed when studying the adsorption of MB and MO on commercial
17 AC [73].

18 The time required to reach equilibrium varies according to the type of micropollutant, the
19 initial concentration and the dose of AC per unit volume of solution. In this study, rapid
20 adsorption kinetics were observed. Some molecules indeed reached equilibrium in only 45
21 min (ATZ), while others required up to 500 min (CIP). Nevertheless, high removal
22 percentages (95 - 100%, as seen in Figure SI 5) were obtained despite the use of a low dose of
23 AC (0.04, 0.2 and 1 g AC/L) and very high initial pollutant concentrations (a few mg/L)
24 compared to those found in tap water (a few $\mu\text{g/L}$). Increasing the dose of AC led to higher
25 elimination percentages and faster achievement of equilibrium.

1 Adsorption kinetics and capacities also depend on the molecular size of micropollutants,
2 which varies considerably. The size of the micropollutants studied varies from 0.85 to 1.32
3 nm in length, from 0.45 to 1.00 nm in width, and from 0.19 to 0.50 nm in height [23].
4 AC850°C-2h (Figure 1 B and Table SI 1) has 33.5% mesopores (2 - 50 nm) and 66.5%
5 micropores (< 2 nm), the latter comprising 54% ultramicropores (< 0.7 nm) and 46%
6 supermicropores (0.7 - 2 nm). These values are consistent with the dimensions of the
7 molecules studied, suggesting that they can be adsorbed irrespective of their orientation.

8 We will then compare classical adsorption kinetics models to determine which one best fits
9 the data. A possible confirmation could be obtained by examining the value of the parameter n
10 of the BSf model, which represents the non-integer order of the reaction.

11 3.2.2. Kinetic studies

12 The adsorption kinetics of micropollutants, studied at room temperature and neutral pH on
13 AC850°C-2h, are shown in Figure 4A for pesticides (ATZ, DEA, ESA MET), Figure 4B for
14 pharmaceuticals (PARA, CBZ, CIP, 17 BE) and Figure 4C for PFAS (PFOS, PFOA and
15 PFHxA). Each curve was fitted by non-linear, PSO, PFO, and BSf models. The parameters of
16 the corresponding kinetic models are summarized in Table SI 3.

17 ATZ adsorption kinetics reaches equilibrium after 45 min of contact. After 60 min, ATZ is
18 completely adsorbed, with an experimental equilibrium adsorbed amount ($q_{e,exp}$) of 9.85 mg/g.
19 This value is closer to that predicted by the PFO model ($q_{e,1} = 9.89$ mg/g) than that predicted
20 by the PSO model ($q_{e,2} = 10.56$ mg/g). Furthermore, the R^2 determination coefficient of the
21 PFO model (0.9995) is significantly higher than that of the PSO model (0.9772), while the χ^2
22 fit error is considerably lower for the PFO model (0.005) than for the PSO model (0.232).
23 These results underline that ATZ adsorption onto AC850°C-2h is a slow process governed by
24 interactions with surface functions as assumed by the PFO model [70,73].

1 Based on the same principle, we carried out a comparative analysis of determination
2 coefficients and fit errors for all the micropollutants studied. The adsorption kinetics of DEA,
3 17 BE and PFOS were found best captured by the PFO model, while the PSO model proved
4 best suited to describe the adsorption kinetics of MET ESA, PARA, CBZ, CIP, PFOA and
5 PFHxA. Although the determination coefficients of the PFO and PSO models did not allow us
6 to favor one specific model, given the similarity of the R^2 values for the different
7 micropollutant kinetics (with the exception of MET ESA and PFHxA, clearly described by the
8 PSO model), application of the BSf model revealed the highest R^2 and lowest χ^2 values.

9 The amounts adsorbed at equilibrium predicted by the BSf model (q_{eBSf}) were indeed
10 found to be closest to experimental values for the various micropollutants studied.
11 Consequently, the BSf model emerged as the most appropriate to describe adsorption kinetics
12 on AC850°C-2h, suggesting a fractal process due to surface heterogeneities, which may be
13 chemical and/or topological in nature. This topological heterogeneity, as revealed by the
14 nitrogen adsorption data used to determine the PSD, manifests in various pore shapes (slits,
15 roughly spherical, cylindrical or bottle-shaped cavities.) and pore diameters. At the same time,
16 the presence of chemical heterogeneity stems from the multiplicity of functional groups on the
17 surface, as confirmed by potentiometric titration.

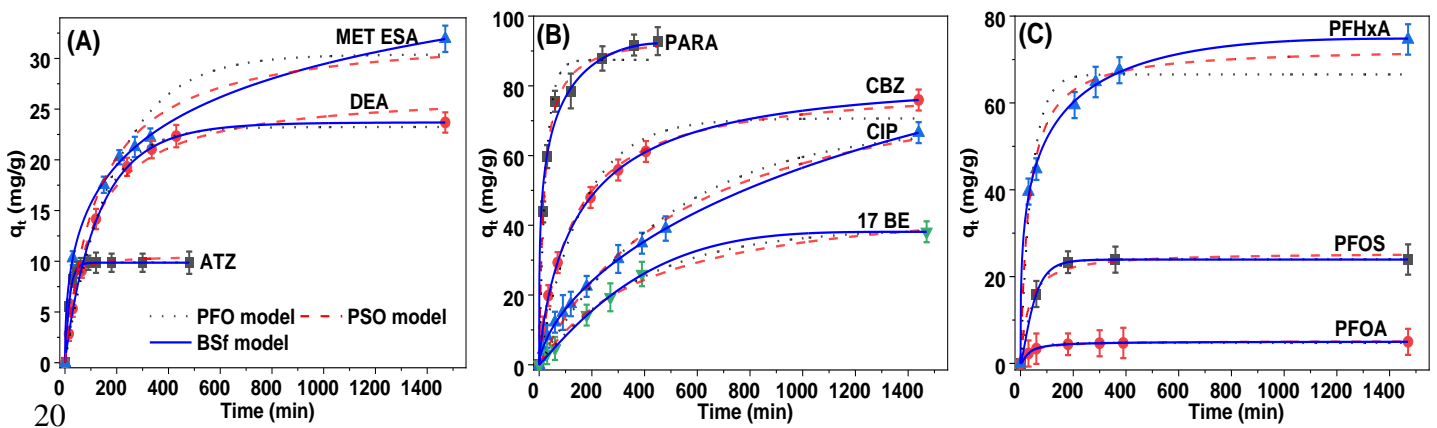
18 The fractional reaction time α , consistently below or close to 1, confirm the fractal nature
19 of the micropollutant adsorption process [73,88,89]. These results are in line with previous
20 research [65,73,89-91]. As demonstrated by Selmi *et al.* [92], fractality and characteristic time
21 τ_c are also influenced by the initial concentration and specific nature of the molecule under
22 study. The parameter τ_c , which varies as a function of the molecule, indicates the point at
23 which adsorption kinetics start to vary slowly considering that equilibrium has been reached,
24 or the necessary time after which kinetic equilibrium should be reached. From this data, it is
25 possible to calculate the time required to adsorb half the initial concentration, known as $\tau_{1/2}$.

1 For example, almost 50% of ATZ molecules are adsorbed after around 13 min (see Figure SI
2 5). This value corresponds closely to $\tau_{1/2}$ (ATZ), estimated at 12.9 min. Similarly, around 50%
3 of 17 BE molecules are adsorbed after around 270 min, matching the $\tau_{1/2}$ value of 258.4 min
4 (see Figure SI 5). For PFHxA molecules, about 50% are adsorbed after approximately 30 min,
5 consistent with the estimated $\tau_{1/2}$ value of 26.8 min (see Figure SI 5).

6 Direct comparison of the adsorption kinetics of the various micropollutants is not possible
7 due to variations in adsorption conditions, in particular the initial concentrations chosen for
8 each micropollutant. These concentrations were chosen according to various factors, such as
9 the detection technique to be used and the solubility of the molecules.

10 Adsorption test results show that wood-based activated charcoal is capable of effectively
11 removing the most common micropollutants found in tap water, despite the use of high initial
12 concentrations and low AC doses. For a more in-depth analysis, a dynamic mode adsorption
13 test, with concentrations of the order of a few $\mu\text{g/L}$, should be considered in a future study.
14 This approach would allow determining the efficiency of synthesized AC under realistic
15 conditions, as well as to establish breakthrough curves and therefore determine the lifetime of
16 the AC with respect to each micropollutant, including the cocktail effect. These conclusions
17 could be reinforced by the study of adsorption isotherms, which would provide a more
18 complete picture of the mechanism by which micropollutants adsorb on AC.

19



1 Figure 4: Adsorption kinetic studies of micropollutants: (A) pesticides; (B) pharmaceuticals;
2 and (C) PFAS on AC850°C-2h, and associated non-linear fits using PSO, PSO and
3 BSf models.

4 3.2.3. Isotherm studies

5 Figure 5 shows the non-linear fits of the adsorption isotherms of the micropollutants
6 studied on AC850°C-2h using the Freundlich, Langmuir, GBS, MLM2E, and DLM2E
7 models. Model parameter values are given in Table SI 4. A general trend was observed for all
8 micropollutants: a significant increase in adsorption capacity with increasing equilibrium
9 concentration, indicating the affinity between the synthesized AC and the studied
10 micropollutants. For DEA, PARA, 17 BE, PFOS and PFOA, a clear plateau is observed once
11 the activated carbon is saturated, while no well-defined plateau is observed in the case of
12 ATZ, MET ESA, CBZ, CIP and PFHxA.

13 A secondary increase in the adsorbed amount as a function of equilibrium concentration is
14 observed for the adsorption isotherms of DEA, ESA MET, CBZ, CIP, PFOS, PFOA, and
15 PFHxA. This can be attributed to the formation of a secondary adsorption layer due to
16 adsorbate-adsorbate interactions, facilitating the attachment of multiple molecules per active
17 site, along with the formation of micelles and aggregates in larger pores. This phenomenon
18 has been reported in several studies [33,57,81,79,93-95] using various adsorbents. For
19 instance, Sellaoui *et al.* [79] modified a commercial AC by chemical treatment with H₂O₂ and
20 annealing at 700 °C under N₂ to study the adsorption of Ibuprofen. They found that the
21 modification increased the number of adsorption layers, suggesting that Ibuprofen molecules
22 aggregate at one site. The sample treated with H₂O₂ showed a higher degree of aggregation,
23 indicating that an oxygenated surface favors the formation of Ibuprofen aggregates. The same
24 phenomenon of multilayer formation was observed by Hanna *et al.* [95] when they studied the

1 adsorption of various PFAS onto AC. They concluded that this adsorption involves multiple
2 interactions between several PFAS molecules and a single active site.

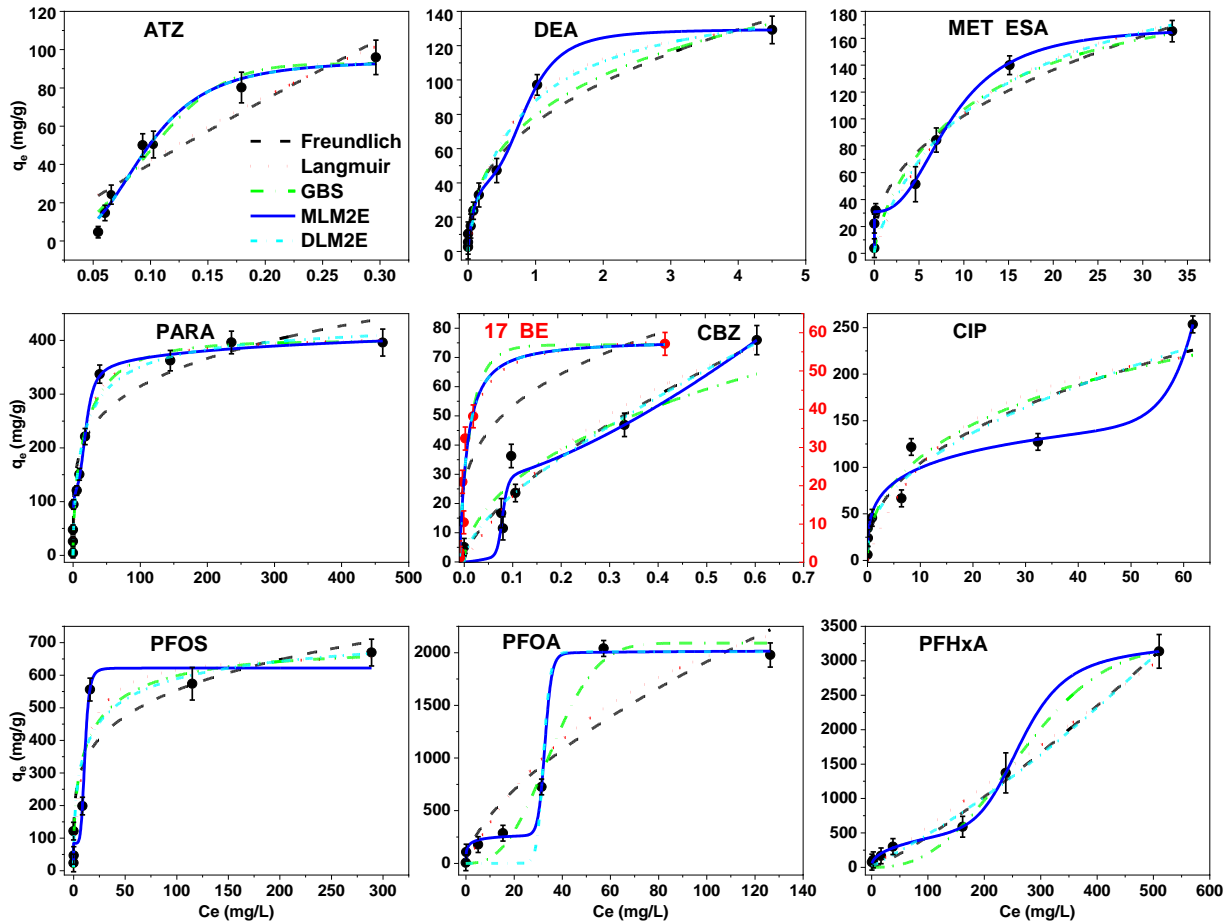
3 The low determination coefficients, R^2 , of the Freundlich model indicate its inability to
4 perfectly describe the adsorption isotherms of micropollutants, particularly at high
5 concentrations where it is prone to errors [96]. The Langmuir model, reliable when saturation
6 is clear, does not describe the isotherms of the micropollutants studied due to incomplete
7 saturation or the formation of several adsorption layers, as confirmed by the low R^2 values
8 (0.7967-0.9723), high χ^2 (40.59-3.45E4), and the significant differences between the
9 maximum experimental adsorbed amounts, $q_{e,max,exp}$, and those predicted by the model.

10 However, the GBS model seems adequate to describe most of the micropollutant isotherms
11 studied, with high R^2 , low χ^2 and $q_{e,max,GBS}$ close to $q_{e,max,exp}$, indicating the stochastic nature
12 (random sequential adsorption due to fractal geometry) of the adsorption process and thus
13 confirming the fractal heterogeneity of the AC surface, as further evidenced by the BSf kinetic
14 model. The GBS model constants, in particular a and c , enable the heterogeneity of the AC
15 surface to be assessed. According to the observations of Selmi *et al.* [73,85,89], when a
16 exceeds 1, as in the case of ATZ, PFOA and PFHxA adsorption, the surface exhibits
17 pronounced topological heterogeneity, allowing several molecules to bind to the same active
18 site. This leads to rapid diffusion of the molecules to the available active sites. On the other
19 hand, when a is less than 1, as in the case of adsorption of other micropollutants, the active
20 sites have different energies, leading to chemical and interface heterogeneities and favoring
21 the formation of successive adsorption layers. These observations suggest that the AC surface
22 is topologically highly heterogeneous, due to its porous structure, characterized by cracks, pits
23 and significant variations in pore size and shape, as highlighted by textural properties results.

24 The c parameter of the GBS model is closely related to the clustering and aggregation of
25 micropollutants, and therefore is a measure of surface heterogeneity. A c value close to 0

1 indicates a very heterogeneous surface, and vice-versa when c is close to 1. Table SI 4 shows
2 that the parameter c approaches 0 for all the micropollutants studied, confirming the fractal
3 distribution demonstrated by the relevance of the BSf kinetic model. Surface heterogeneity
4 can result from topological and chemical characteristics. Interface heterogeneity can result
5 from the aggregation of micropollutant molecules on the adsorbent-adsorbate interface.
6 However, it is essential to note that the GBS model has limitations in its ability to describe
7 certain adsorption isotherms, particularly when these do not reach a clear equilibrium,
8 especially in the case of isotherms with several adsorption layers [77,97]. The formation of
9 multiple adsorption layers, or the binding of molecules to different types of active sites, can
10 be analyzed using adsorption isotherm models based on statistical physics [79].

11 As shown in Figure 5, adsorption isotherms were fitted with two models derived from
12 statistical physics, namely MLM2E and DLM2E, which are particularly suitable for isotherms
13 exhibiting multilayer adsorption processes (DEA, MET ESA, CBZ, CIP, PFOS, PFOA and
14 PFHxA). It should be noted that the MLM2E model stands out as the one that best describes
15 micropollutant adsorption isotherms, probably due to the high number of parameters (6) it
16 includes.



1
2

3 Figure 5: Non-linear fits of the adsorption isotherms of micropollutants studied on
4 AC850°C2h using various models.

5 The performance of these models, particularly MLM2E, is reflected in high coefficients of
6 determination (R^2), low χ^2 values, and maximum adsorption capacities ($q_{e,max}$) very close to
7 experimental values ($q_{e,max,exp}$). Despite the good fit of CIP and PFHxA isotherms by the
8 MLM2E model, characterized by high R^2 values (0.9595 and 0.9985, respectively) as
9 observed in Figure 5, there is a significant disparity between the experimental maximum
10 adsorbed amounts ($q_{e,max,exp}$ of 253 and 3135 mg/g, respectively) and the total maximum
11 adsorbed amounts predicted by the model ($q_{e,max,MLM2E}$ of $6.67 \cdot 10^8$ and $5.06 \cdot 10^5$ mg/g,
12 respectively). Calculating the maximum adsorbed amounts of CIP for each type (1 and 2) of
13 active site ($q_{emax1} = n_1 D_1$ and $q_{emax2} = n_2 D_2$, determined by MLM2E), we found a q_{emax1} of
14 315 mg/g, closer to the experimental value ($q_{e,max,exp}(CIP) = 253$ mg/g) than q_{emax2} , which is

1 equal to $6.67 \cdot 10^8$ mg/g. This result indicates that the significant disparity is due to the type-2
2 sites and suggests that CIP molecules are primarily adsorbed by type-1 sites rather than type-2
3 sites. Similarly, for PFHxA, $q_{e \max 2} = 2329$ mg/g, close to $q_{e, \max, \exp}$ (3135 mg/g). This
4 observation indicates that PFHxA molecules are preferentially adsorbed by type-2 sites rather
5 than type-1 sites. Similar results can be extended to the adsorption of ATZ and 17 BE since
6 their n_1 and n_2 values are zero, respectively. In these cases, the $q_{e \max, \exp}$ of ATZ (95.95 mg/g)
7 is much closer to $q_{e \max 2}$ (94.25 mg/g) than $q_{e \max 1}$ (0 mg/g), while the $q_{e \max, \exp}$ of 17 BE
8 (57.07 mg/g) is much closer to $q_{e \max 1}$ (58.07 mg/g) than $q_{e \max 2}$ (0 mg/g). This indicates that
9 each molecule is primarily adsorbed by one type of site rather than others, depending on the
10 energy of the adsorption site. For a more in-depth discussion of the different “ n scenarios”,
11 see below, we will consider only n_1 for the adsorption of CIP and 17 BE, and n_2 for the
12 adsorption of ATZ and PFHxA.

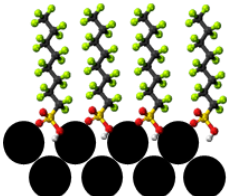
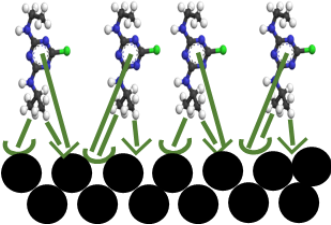
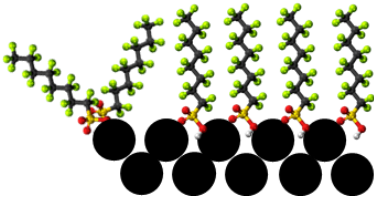
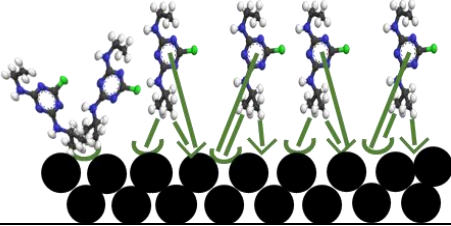
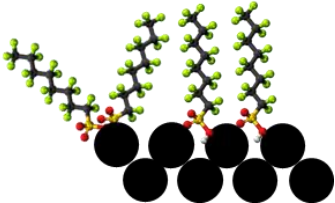
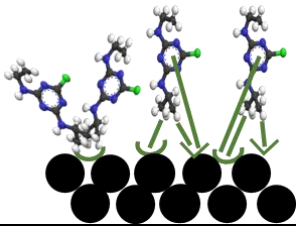
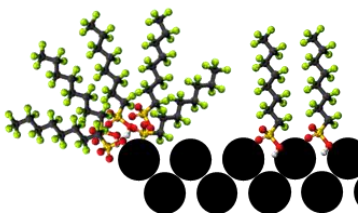
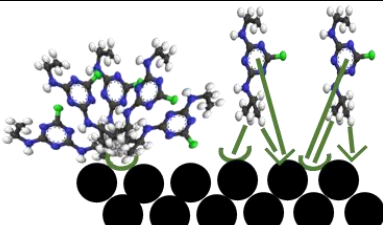
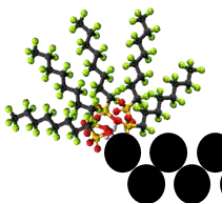
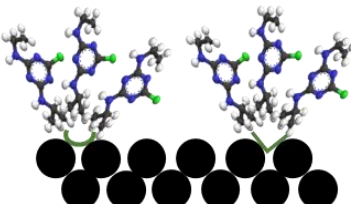
13 Several studies [33,81,82,98] included the parameter n , corresponding to the number of
14 molecules adsorbed per adsorption site, when using the MLM2E and DLM2E models to
15 characterize the anchoring geometry of micropollutants on the AC surface, as well as their
16 degree of molecular aggregation in solution. Three potential scenarios can be outlined, as
17 illustrated in Table 2 **Erreur ! Source du renvoi introuvable.**:

- 18 • For $n < 0.5$: there are two or more active sites for pollutant binding, with parallel
19 anchoring. The adsorption process involves multiple interactions;
- 20 • For $0.5 < n < 1$: this is the domain of mixed-anchoring adsorption. Micropollutants can
21 be captured by one or two active sites, in varying proportions. If $0.5 < n < 0.75$,
22 interaction with two adsorption sites predominates, while for $n = 0.75$, interactions at
23 one or two sites are equivalent. For $n > 0.75$, interaction is predominant at a single
24 site;

- 1 • For $n > 1$: molecules attach in a non-parallel anchoring, where a single active site
- 2 interacts with several molecules. This is the principle of multi-molecular adsorption.

3

4 Table 2: Interaction scenarios between molecules and active sites as function of n .

n	Sorption interaction with the carbon surface	Sorption interaction with surface functional groups	Sorption mechanisms
$n \leq 0.5$			<ul style="list-style-type: none"> - Two or more active sites for pollutant binding - Parallel anchoring - Adsorption with multiple interactions
$0.5 < n < 0.75$			<ul style="list-style-type: none"> - Mixed-anchoring adsorption - Interaction with two adsorption sites predominates
$n = 0.75$			<ul style="list-style-type: none"> - Mixed-anchoring adsorption - Interactions at one or two sites are equivalent
$0.75 < n \leq 1$			<ul style="list-style-type: none"> - Mixed-anchoring adsorption - Interaction with one adsorption sites predominates
$n > 1$			<ul style="list-style-type: none"> - A single active site interacts with several molecules. - Non-parallel anchoring - Multi-molecular adsorption with cluster formation

5

6 Table SI 4 reveals that $n_1 < 0.5$ for PARA (0.15) and CIP (0.36), indicating that the

7 molecules of these two micropollutants were anchored parallel to each other through multiple

8 interactions with two or more type-1 active sites. In the case of PFOA adsorption, n_1 (0.51)

1 lies between 0.5 and 0.75, suggesting mixed anchoring of PFOA molecules to two or more
2 adsorption sites via multiple interactions. The parameter n_1 for DEA, MET ESA, CBZ, 17 BE,
3 and PFOS, as well as the parameter n_2 for all micropollutants (with the exception of CIP and
4 17 BE, which are not considered for the reasons mentioned above) are greater than 1. This
5 indicates that several molecules are adsorbed in a non-parallel manner by a single type-1
6 and/or type-2 active site. This multi-molecular adsorption leads to the formation of aggregates
7 (assembly of molecules) on the active sites, resulting in the formation of several adsorption
8 layers, as illustrated by DEA, MET ESA, CBZ, CIP, PFOA, PFOS and PFHxA isotherms in
9 Figure 5.

10 The high n_2 values for DEA, MET ESA, PFOS, PFOA and PFHxA molecules (3.64, 4.18,
11 5.30, 23.37 and 6.96, respectively) explain their high experimentally adsorbed amounts (129,
12 165, 669, 1977 and 3134 mg/g). This phenomenon may also explain the formation of a second
13 adsorption layer for these micropollutants, as observed for CBZ, which has an n_1 of 14, thus
14 confirming the molecule aggregation already suggested by the c parameter of the GBS model.
15 Interestingly, n_2 values are higher than n_1 for all micropollutants. It is therefore reasonable to
16 conclude that type-2 active sites are better able to bind molecules than type-1 active sites, and
17 that since n_2 (number of molecules adsorbed by type 2 sites) $> n_1$, then type-2 sites are able to
18 adsorb molecules better than type-1 sites.

19 As mentioned, adsorption isotherms correspond to monolayers in the case of ATZ, PARA
20 and 17 BE, indicating that these molecules are bound by a dominant adsorption mechanism.
21 In contrast, multilayer adsorption is observed for DEA, MET ESA, CBZ, CIP and the three
22 PFAS, suggesting the existence of several simultaneous adsorption mechanisms. These
23 possible adsorption mechanisms for each micropollutant are examined in the next section.

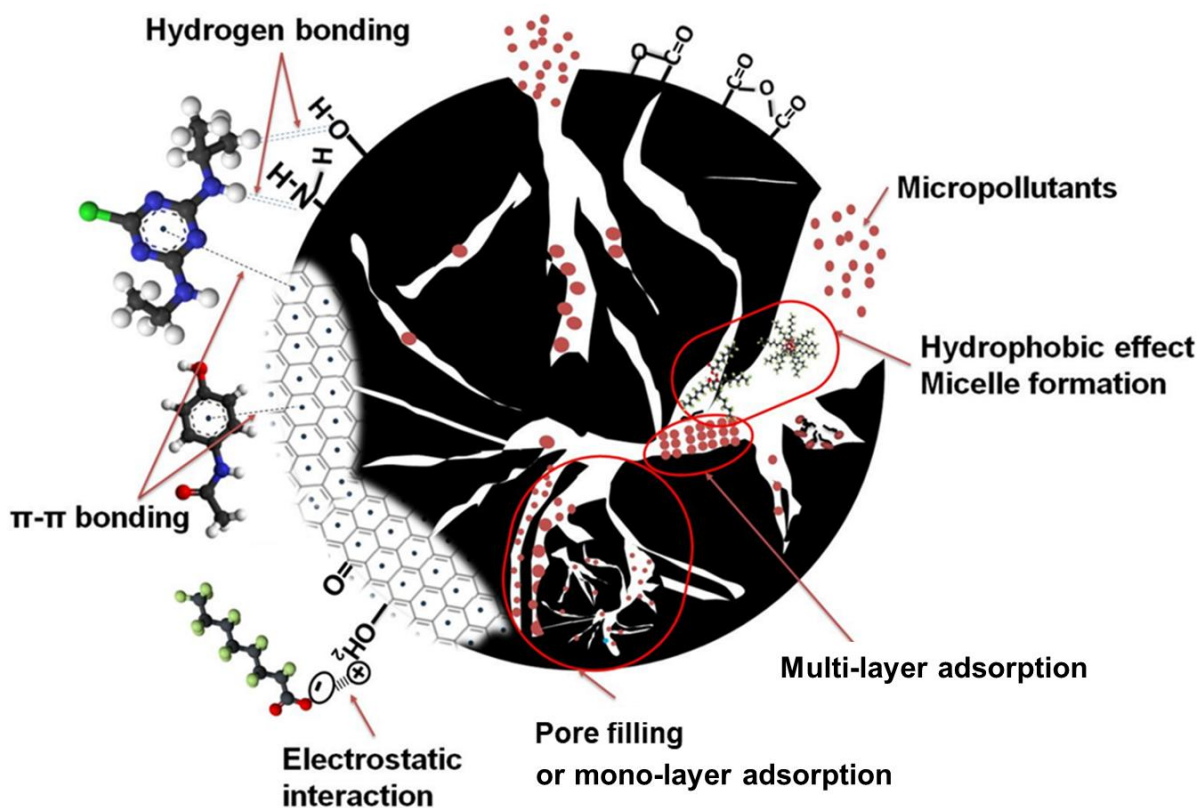
24

25

1 3.2.4. *Possible adsorption mechanisms of micropollutants*

2 Micropollutants adsorb onto AC by several mechanisms. These mechanisms include pore
3 filling, electrostatic interactions, hydrogen bonding, Van der Waals interactions, π - π and CH- π
4 bonding, and the hydrophobic effect. Details of these mechanisms are available in a previous
5 work [23]. Adsorption mechanisms are influenced by several parameters, such as adsorption
6 operating conditions (pH, temperature: fixed in our case), physicochemical characteristics of
7 the ACs (A_{BET} , PSD, pH_{PZC} , amount and nature of surface functions: fixed in our case since
8 only one adsorbent is tested) and physicochemical characteristics of the micropollutants (size,
9 charges, solubility, hydrophobicity...). To determine the predominant adsorption mechanisms
10 for the micropollutants studied, an in-depth analysis of these characteristics is required.

11 Figure 6 summarizes the various possible adsorption mechanisms for the micropollutants
12 studied. The dimensions of the micropollutants studied, already provided in Section 3.2.1,
13 perfectly enable the pores of AC to be penetrated, whatever the orientation of the molecule
14 under consideration. In addition, the porous structure of AC can be filled with more than one
15 molecule, which explains the formation, or initiation, of multilayer adsorption.



1
2 Figure 6: Possible micropollutant adsorption mechanisms on activated carbon.

3 The pH_{PZC} of AC850°C2h is 9.31. If the pH of the solution remains below pH_{PZC} , the
4 surface of the AC is positively charged, which favors the adsorption of negatively charged
5 micropollutants such as MET ESA, PFOS, PFOA and PFHxA via electrostatic interactions
6 with the positive charges of AC surface functions such as $-OH_2^+$, $-NH_3^+$, $\Phi=OH^+$. [99].
7 Furthermore, the hydrophobicity of these molecules enhances their adsorption through
8 hydrophobic effect, forming micelles and hemi-micelles within large pores by Van der Waals
9 interaction with the hydrophobic surfaces of the AC. These clusters and aggregations (micelle
10 and hemi-micelle formation) were indicated by the parameter c in the GBS model and n of the
11 MLM2E model. This may explain the multi-layer adsorption process of these molecules, as
12 confirmed by our study and others [95,100,101].

13 However, for micropollutants such as ATZ, DEA, PARA, CBZ, CIP and 17 BE, which are
14 uncharged molecules in the water pH range 6.5 to 9.5, Van der Waals interaction may

1 predominate over electrostatic interaction [30,102,103]. These micropollutants have the
2 ability to form hydrogen bonds with AC surface functions (*e.g.* nitrogen or oxygen-based
3 functional groups) or with other adsorbed molecules, thus initiating multilayer formation.
4 Adsorption of neutral micropollutants can lead to electron delocalization, promoting the
5 formation of additional chemical bonds and thus multilayer adsorption, as has been observed
6 for DEA, CBZ and CIP. PFAS contain hydrophobic C-F chains that repel water molecules.
7 Oxygen atoms contained in PFAS functional groups act as electron acceptors in hydrogen
8 bonding with NH, OH. groups. Oxygen-containing functional groups can capture water
9 molecules by hydrogen bonding from solution, resulting in competitive sorption of water with
10 PFAS [99]. Finally, the presence of aromatic rings in all the micropollutants studied, with the
11 exception of PFAS, also enables the establishment of π - π interactions between the π electrons
12 of their aromatic rings and those of the aromatic rings of ACs and their surface functions such
13 as phenolic groups, lactones, quinones. [32,104-106].

14 Given the complexity of adsorption on AC, characterized by diverse pore sizes, surface
15 groups, and charge variations according to environmental conditions, no single mechanism
16 can be favored over another. An integrated approach considering all these factors is thus
17 needed to fully understand the adsorption process and optimize the efficiency of contaminated
18 water treatment.

19 3.2.5. *Comparative studies of micropollutants adsorption*

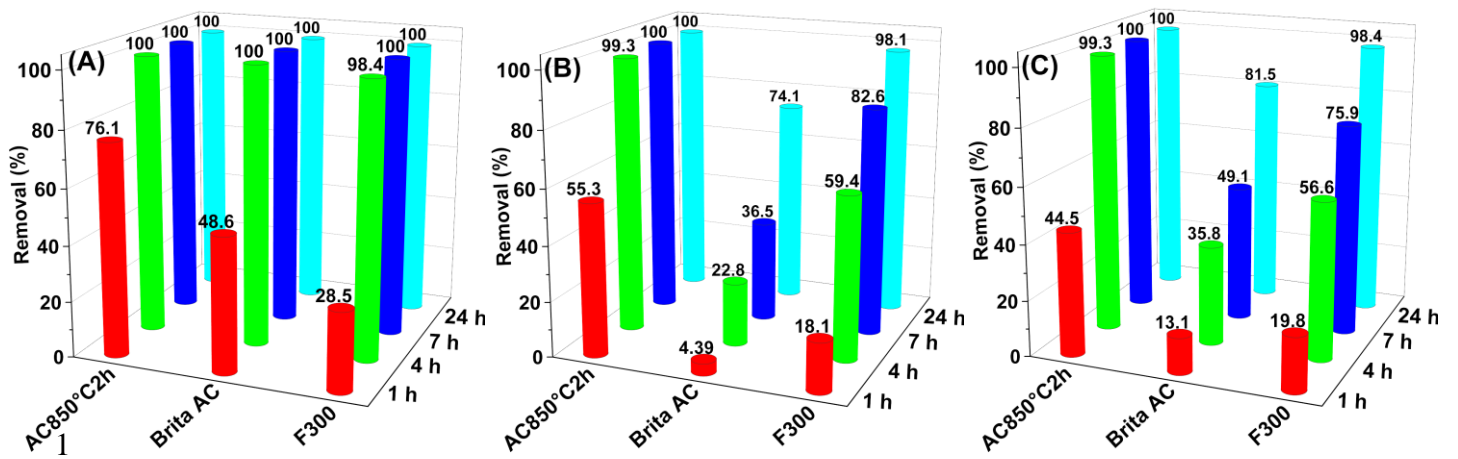
20 To assess the performance of the synthesized AC compared with the two commercially
21 available ACs introduced above, the coconut-shell AC used in Brita filter carafes (Brita AC)
22 and the coal-based AC FiltraSorb 300 (F300) from Calgon Carbon, a series of adsorption tests
23 was carried out. Physicochemical characterization and adsorption tests were performed at
24 different initial concentrations of atrazine (ATZ), *i.e.*, 1, 5 and 10 mg/L. Adsorption
25 efficiencies were measured at predefined time intervals, *i.e.*, 1, 4, 7 and 24 h, in order to

1 elucidate the adsorption kinetics for each adsorbent, including AC850°C-2h. Figure 7 shows
2 ATZ removal (%) as a function of time and initial concentration for the three adsorbents.

3 At a low ATZ concentration (1 mg/L), AC850°C-2h had the highest adsorption capacity
4 after 1 h, outperforming Brita AC by 1.5 times and F300 by 2.7 times. However, it is
5 important to note that Brita AC exhibits rapid saturation and limited efficacy despite its A_{BET}
6 (1025 m²/g) close to that of AC850°C-2h (1110 m²/g). At high initial ATZ concentrations (5
7 and 10 mg/L), AC850°C-2h clearly stood out, achieving 99.3% ATZ elimination after just 4 of
8 contact, while F300 and Brita AC achieved elimination rates of 98.4% and 81.5% after 24
9 hours, respectively. This underlines the remarkable speed and efficiency of AC850°C-2h
10 compared to Brita AC and F300.

11 F300 showed a higher ATZ adsorption capacity than Brita AC, despite its lower A_{BET} (855
12 m²/g). This observation suggests that other characteristics, such as pore size distribution and
13 functional groups, may play a crucial role in contaminant adsorption efficiency. Given that the
14 total amount of basic functions of F300 and Brita AC are similar (0.53 and 0.51 mmol/g
15 respectively), and that Brita AC exhibits a greater diversity of surface functions, the
16 pronounced difference in adsorption performance between Brita AC and AC850°C-2h, despite
17 comparable BET areas, is attributed to their distinct pore size distribution. Whereas Brita AC
18 is primarily microporous with a limited mesoporous fraction (9%), F300 has well-developed
19 mesoporosity (26%), which favors efficient and rapid adsorption of ATZ.

20 AC850°C-2h is the most effective and faster ATZ adsorbent, whatever the initial
21 concentration and contact time. This is due to its adequate BET area and pore size
22 distribution, as well as the presence of appropriate surface functions, such as basic oxygen
23 groups (pyrones) and amine functions (pyridines), as reported in our published study [23].
24 AC850°C-2h has an amount of basic and acidic functions of 0.69 mmol/g and 0.15 mmol/g,
25 respectively.



2 Figure 7: ATZ removal by AC850°C-2h compared with Brita AC and F300 commercial ACs
 3 at different contact times and initial concentrations: (A) $C_i = 1$ mg/L; (B) $C_i = 5$
 4 mg/L; and (C) $C_i = 10$ mg/L.

5 A comparative analysis of the maximum adsorption capacities ($q_{e,max}$), summarized in Table
 6 SI 6, was carried out with ACs reported in the literature. This comparison considers operating
 7 conditions such as AC dosage and BET area, initial micropollutant concentration (C_i) and
 8 contact time. The results are based on experiments carried out at 25 °C and pH 7.3. With
 9 regard to ATZ adsorption, AC850°C-2h performed 4.5 times better than PCPAC, which was
 10 obtained by chemical activation with $FeCl_3$ of Araca fruit husks, despite using a dose five
 11 times higher. This can be explained by its lower A_{BET} (431 m^2/g) and shorter contact time (3
 12 h). The maximum concentration ($C_{i,max}$) of ATZ used here is 40 mg/L, which slightly exceeds
 13 its solubility in water (33 to 35 mg/L at 25°C) [107].

14 DEA adsorption was studied by Faur *et al.* [108], using AC fiber (ACF RS 1301) produced
 15 by Actitex Companies (Levallois, France) using steam activation of Rayon. Higher $q_{e,max}$ (150
 16 mg/g) and higher A_{BET} (1461 m^2/g) were found compared to our work ($q_{e,max}$ of 129 mg/g).
 17 This could be attributed to the fibrous structure of this AC, offering a greater contact area with
 18 DEA, as well as a better adsorption kinetics and longer contact time (48 h versus 24 h in our
 19 study).

1 MET ESA adsorption was carried out by Gomis-Berenguer *et al.* (2021) [103], who
2 synthesized two ACs (S-KC and R-KC) by chemical activation with K_2CO_3 of lignocellulosic
3 precursors, sunflower seed hulls and rapeseed straw, respectively. These ACs exhibited
4 exceptionally high A_{BET} of 2024 and 2220 m^2/g , respectively. Consequently, they achieved
5 higher $q_{e,max}$ of 218 mg/g and 273 mg/g, compared to 165 mg/g for AC850°C-2h. In the same
6 study, AQ630 (commercial AC from Jacobi France), with an A_{BET} of 1016 m^2/g comparable to
7 that of AC850°C-2h, exhibited a $q_{e,max}$ (ESA MET) of 93 mg/g, which is significantly lower
8 than that of AC850°C-2h.

9 PARA adsorption was studied by Melliti *et al.* [44], in which AAC and PC, produced by
10 $ZnCl_2$ chemical activation of artichoke leaves and pomegranate peel, respectively, were used
11 as adsorbents and showed A_{BET} of 1203 and 1095 m^2/g , respectively. Although textural
12 properties were similar to that of AC850°C-2h, lower adsorption capacities (215 and 143
13 mg/g) were measured compared with that of AC850°C-2h (396 mg/g), despite higher doses,
14 lower initial concentrations and a contact time of 24 h. This indicates that, in addition to
15 textural properties, AC850°C-2h presents other factors influencing adsorption capacities, such
16 as the surface functional groups. This can be confirmed by the CBZ adsorption by ACMW,
17 which is an AC produced by KOH chemical activation and microwave pyrolysis of primary
18 sludge from the paper industry. ACMW was then doped with different iron II fractions to
19 produce MACX3. Maximum adsorbed amounts were 198 and 134 mg/g, respectively,
20 exceeding that of AC850°C-2h, which is 76 mg/g. This is remarkable despite the lower (795
21 m^2/g) or similar (1082 m^2/g) A_{BET} of MACX3 and ACMW, respectively, compared to that of
22 AC850°C-2h, as well as the significantly lower dose and contact time. ACMW presents a total
23 pore volume V_{tot} of 0.79 cm^3/g , higher than that of AC850°C2h (0.63 cm^3/g). In addition,
24 MACX3 and ACMW are rich in oxygen functionalities: carbonyl, carboxyl, quinone and
25 ketone groups.

1 With regard to CIP adsorption, AC850°C-2h demonstrated a slightly higher $q_{e,max}$ (253
2 mg/g) compared to GAC (221 mg/g), even though a higher dose of GAC (1.1 g/L) was used
3 with the same contact time and C_i interval. Here, GAC refers to a commercial AC produced
4 by Jalmek (Mexico) by chemical activation of lignocellulose with phosphoric acid. This
5 difference may be attributed to the slightly lower A_{BET} of GAC (940 m²/g) compared with
6 AC850°C-2h, or to the presence of suitable surface functional groups that facilitate CIP
7 removal from water.

8 Finally, concerning PFAS adsorption, BC-P(SB-co-AM), which is a biochar prepared by
9 slow pyrolysis of wood chips and doped with quaternary ammonium groups, has an
10 adsorption capacity of 536 mg/g for PFOA and 634 mg/g for PFOS. In comparison,
11 AC850°C2h, with an A_{BET} of 1110 m²/g, has a PFOS adsorption capacity of 669.5 mg/g, very
12 close to that of BC-P(SB-co-AM) despite its low BET area of 167 m²/g. This demonstrates the
13 importance of surface functions, particularly amine functions, in the selective and efficient
14 adsorption of PFAS. Overall, adsorbents with a higher A_{BET} do not always guarantee better
15 $q_{e,max}$ adsorption capacity for all pollutants. Performance also depends on the chemical
16 properties (pH_{PZC} and surface functions) of the ACs, as well as on the nature of the pollutant,
17 its initial concentration, the dose of adsorbent and the contact time.

18

19 **4. Conclusion**

20 Groupe Bordet's wood-based charcoal was converted into highly porous activated carbon
21 (AC) through physical activation with steam in a rotary kiln. Increasing time and temperature
22 led to the creation of micropores that gradually evolved into mesopores. The AC synthesized
23 at 850 °C for 2 hours, with a BET surface area exceeding 1100 m²/g and a micro-mesoporous
24 structure with over 30% mesoporosity, showed promise for tap water purification, due to its
25 optimized textural properties, which support effective micropollutant adsorption. Comparative

1 studies with commercial ACs demonstrated that our optimized AC surpasses others, largely
2 due to its well-developed mesoporosity. This finding highlights the crucial role of mesopores
3 in enhancing adsorption efficiency, complementing micropores by providing numerous active
4 sites and speeding up adsorption kinetics, which leads to excellent performance even at short
5 contact times.

6 Kinetic studies, described by the BSf model, revealed a rapid, fractal adsorption process,
7 indicating surface heterogeneity and active site accessibility. Adsorption isotherms
8 highlighted multilayer adsorption behavior for specific micropollutants, including DEA, MET
9 ESA, CBZ, CIP, and three PFAS molecules. Pore filling, Van der Waals interactions, and
10 hydrogen bonding were identified as primary adsorption mechanisms for all the
11 micropollutants studied. Interestingly, only PFAS and MET ESA can be adsorbed by
12 electrostatic interactions and hydrophobic effects, while pesticide and drug molecules can be
13 adsorbed by π - π interactions. Future research will focus on increasing the density of
14 AC850°C2h by compaction using a bio-based binder, conducting AC regeneration
15 experiments to evaluate durability, performing dynamic adsorption tests under real-world
16 conditions, and working to improve the adsorption selectivity for challenging micropollutants,
17 such as short-chain PFAS.

18

19 **Acknowledgements**

20 The authors would like to thank the France Relance program for its financial support under
21 grant n°ANR-21-PRRD-0053-01.

22

23

1 References

- 2 1. Stockholm, Convention: What are Persistent Organic Pollutants (POPs)?
3 <https://www.pops.int/TheConvention/ThePOPs/tabid/673/Default.aspx> (2019).
- 4 2. Anses: Scientific and technical support report - Laboratory work programme 2020-2022 :
5 National campaign to measure the occurrence of emerging compounds in water
6 destined for human consumption : Pesticides and pesticide metabolites - Explosive
7 residues 1,4-dioxane. Anses: French Ministry of Health and Prevention **85**(2), 1-85
8 (2023). doi:<https://www.anses.fr/fr/system/files/LABORATOIRE2022AST0255Ra.pdf>
- 9 3. Anses: National campaign of occurrence of perfluorinated alkyl compounds in water
10 destined for human consumption. Anses: French Ministry of Health and Prevention
11 **120**(1), 1-120 (2011). doi:<https://sante.gouv.fr/IMG/pdf/rap0511-2.pdf>
- 12 4. Boiteux, V., Dauchy, X., Rosin, C., Munoz, J.-F.: National Screening Study on 10
13 Perfluorinated Compounds in Raw and Treated Tap Water in France. Archives of
14 Environmental Contamination and Toxicology **63**(1), 1-12 (2012).
15 doi:10.1007/s00244-012-9754-7
- 16 5. Anses: AVIS de l'Agence nationale de sécurité sanitaire de l'alimentation, de
17 l'environnement et du travail relatif à l'évaluation des risques sanitaires d'alkyls per-
18 et polyfluorés dans les eaux destinées à la consommation humaine. Anses: French
19 Ministry of Health and Prevention **55**(Saisine n° 2015-SA-0105), 1-55 (2017).
20 doi:<https://www.anses.fr/fr/system/files/EAUX2015SA0105.pdf>
- 21 6. Le Coadou, L., Le Ménach, K., Labadie, P., Dévier, M.-H., Pardon, P., Augagneur, S.,
22 Budzinski, H.: Quality survey of natural mineral water and spring water sold in
23 France: Monitoring of hormones, pharmaceuticals, pesticides, perfluoroalkyl
24 substances, phthalates, and alkylphenols at the ultra-trace level. Sci Tot Environ **603-
25 604**, 651-662 (2017). doi:<https://doi.org/10.1016/j.scitotenv.2016.11.174>
- 26 7. Dauchy, X.: Per- and polyfluoroalkyl substances (PFASs) in drinking water: Current state
27 of the science. Current Opinion in Environmental Science & Health **7**, 8-12 (2019).
28 doi:<https://doi.org/10.1016/j.coesh.2018.07.004>
- 29 8. Anses: Campagne nationale d'occurrence des résidus de médicaments dans les eaux
30 destinées à la consommation humaine: Ressources en eaux brutes et eaux traitées.
31 Etude scientifique Janvier (2011).
- 32 9. Danner, M.-C., Robertson, A., Behrends, V., Reiss, J.: Antibiotic pollution in surface fresh
33 waters: Occurrence and effects. Sci Tot Environ **664**, 793-804 (2019).
34 doi:<https://doi.org/10.1016/j.scitotenv.2019.01.406>
- 35 10. Charraud, L., Jardé, E., Jaffrézic, A., Liotaud, M., Goyat, Q., Mercier, F., Le Bot, B.:
36 Veterinary pharmaceutical residues in water resources and tap water in an intensive
37 husbandry area in France. Sci Tot Environ **664**, 605-615 (2019).
38 doi:<https://doi.org/10.1016/j.scitotenv.2019.01.303>
- 39 11. Lévi, Y.: Contamination des eaux par les résidus de médicaments et stratégies de
40 prévention. Actualités Pharmaceutiques **59**(594), 18-23 (2020).
41 doi:<https://doi.org/10.1016/j.actpha.2020.01.007>
- 42 12. Zango, Z.U., Garba, A., Haruna, A., Imam, S.S., Katsina, A.U., Ali, A.F., Abidin, A.Z.,
43 Zango, M.U., Garba, Z.N., Hosseini-Bandegharai, A., Yuguda, A.U., Adamu, H.: A
44 systematic review on applications of biochar and activated carbon derived from
45 biomass as adsorbents for sustainable remediation of antibiotics from pharmaceutical
46 wastewater. Journal of Water Process Engineering **67**, 106186 (2024).
47 doi:<https://doi.org/10.1016/j.jwpe.2024.106186>
- 48 13. Ashley, S., Helen, G., Julia, D., Pamela, S.: Pharmaceutical Water Screening Values
49 Report : Methods and Results of Rapid Assessments for Pharmaceuticals, Drinking

- 1 Water Contaminants of Emerging Concern Program. Minnesota Department of Health
2 : Health Risk Assessment Unit **57**(1), 1-57 (2015).
3 doi:<https://www.health.state.mn.us/communities/environment/risk/docs/guidance/dwe>
4 [c/pharmwaterrept.pdf](https://www.health.state.mn.us/communities/environment/risk/docs/guidance/dwe/c/pharmwaterrept.pdf)
- 5 14. Chain, E. Panel o.C.i.t.F., Schrenk, D., Bignami, M., Bodin, L., Chipman, J.K., del Mazo,
6 J., Grasl-Kraupp, B., Hogstrand, C., Hoogenboom, L., Leblanc, J.-C., Nebbia, C.S.,
7 Nielsen, E., Ntzani, E., Petersen, A., Sand, S., Vleminckx, C., Wallace, H., Barregård,
8 L., Ceccatelli, S., Cravedi, J.-P., Halldorsson, T.I., Haug, L.S., Johansson, N., Knutsen,
9 H.K., Rose, M., Roudot, A.-C., Van Loveren, H., Vollmer, G., Mackay, K., Riolo, F.,
10 Schwerdtle, T.: Risk to human health related to the presence of perfluoroalkyl
11 substances in food. *EFSA Journal* **18**(9), e06223 (2020).
12 doi:<https://doi.org/10.2903/j.efsa.2020.6223>
- 13 15. Minnesota Department of Health: Toxicological Summary for: Metolachlor ESA CAS:
14 171118-09-5. Health Risk Limits for Groundwater, Health Risk Assessment Unit,
15 Environmental Health Division **4**(651-201-4899), 1-4 (2020).
16 doi:<https://www.health.state.mn.us/communities/environment/risk/docs/guidance/gw/>
17 [metolachloresasumm.pdf](https://www.health.state.mn.us/communities/environment/risk/docs/guidance/gw/metolachloresasumm.pdf)
- 18 16. Minnesota Department of Health: Toxicological Summary for: Cyanazine and Atrazine
19 Chlorinated Degradates. Health Risk Limits for Groundwater, Health Risk Assessment
20 Unit, Environmental Health Division **4**(651-201-4899), 1-4 (2020).
21 doi:<https://www.health.state.mn.us/communities/environment/risk/docs/guidance/gw/c>
22 [yanatradegs.pdf](https://www.health.state.mn.us/communities/environment/risk/docs/guidance/gw/c/yanatradegs.pdf)
- 23 17. Minnesota Department of Health: Toxicological Summary for: Perfluorooctanoate. Health
24 Risk Limits for Groundwater, Health Risk Assessment Unit, Environmental Health
25 Division **14**(651-201-4899), 1-14 (2020).
26 doi:<https://www.health.state.mn.us/communities/environment/risk/docs/guidance/gw/p>
27 [foa.pdf](https://www.health.state.mn.us/communities/environment/risk/docs/guidance/gw/p/foa.pdf)
- 28 18. Minnesota Department of Health: Toxicological Summary for: Perfluorooctane sulfonate.
29 Health Risk Limits for Groundwater, Health Risk Assessment Unit, Environmental
30 Health Division **19**(651-201-4899), 1-19 (2020).
31 doi:<https://www.health.state.mn.us/communities/environment/risk/docs/guidance/gw/p>
32 [fos.pdf](https://www.health.state.mn.us/communities/environment/risk/docs/guidance/gw/p/fos.pdf)
- 33 19. Minnesota Department of Health: Toxicological Summary for: 17 α -Ethinylestradiol.
34 Health Risk Limits for Groundwater, Health Risk Assessment Unit, Environmental
35 Health Division **89**(651-201-4899), 1-9 (2020).
36 doi:<https://www.health.state.mn.us/communities/environment/risk/docs/guidance/gw/e>
37 [thinylestsumm.pdf](https://www.health.state.mn.us/communities/environment/risk/docs/guidance/gw/e/thinylestsumm.pdf)
- 38 20. Minnesota Department of Health: Toxicological Summary for: Perfluorohexanoate. Health
39 Risk Limits for Groundwater, Health Risk Assessment Unit, Environmental Health
40 Division **8**(651-201-4899), 1-8 (2021).
41 doi:<https://www.health.state.mn.us/communities/environment/risk/docs/guidance/gw/p>
42 [fhxa.pdf](https://www.health.state.mn.us/communities/environment/risk/docs/guidance/gw/p/fhxa.pdf)
- 43 21. Minnesota Department of Health: Human Health-Based Water Guidance Table :health-
44 based rules and guidance to evaluate potential human health risks from exposures to
45 chemicals in groundwater. In: Health Risk Limits for Groundwater, Health Risk
46 Assessment Unit, Environmental Health Division. (2023)
- 47 22. Inserm: Pesticides et effets sur la santé : Nouvelles données. Collection Expertise
48 collective. Montrouge : EDP Sciences. **1036**(1), 1-1036 (2021).
49 doi:[https://www.inserm.fr/wp-content/uploads/2021-07/inserm-expertisecollective-](https://www.inserm.fr/wp-content/uploads/2021-07/inserm-expertisecollective-pesticides2021-rapportcomplet-0.pdf)
50 [pesticides2021-rapportcomplet-0.pdf](https://www.inserm.fr/wp-content/uploads/2021-07/inserm-expertisecollective-pesticides2021-rapportcomplet-0.pdf)

- 1 23. Selmi, T., Gentil, S., Fierro, V., Celzard, A.: Key factors in the selection, functionalization
2 and regeneration of activated carbon for the removal of the most common
3 micropollutants in drinking water. *J Environ Chem Eng* **12**(4), 113105 (2024).
4 doi:<https://doi.org/10.1016/j.jece.2024.113105>
- 5 24. Zango, Z.U., Ethiraj, B., Al-Mubaddel, F.S., Alam, M.M., Lawal, M.A., Kadir, H.A.,
6 Khoo, K.S., Garba, Z.N., Usman, F., Zango, M.U., Lim, J.W.: An overview on human
7 exposure, toxicity, solid-phase microextraction and adsorptive removal of
8 perfluoroalkyl carboxylic acids (PFCAs) from water matrices. *Environmental*
9 *Research* **231**, 116102 (2023). doi:<https://doi.org/10.1016/j.envres.2023.116102>
- 10 25. Garba, Z.N., Abdullahi, A.K., Haruna, A., Gana, S.a.A.: Risk assessment and the
11 adsorptive removal of some pesticides from synthetic wastewater: a review. *Beni-Suef*
12 *University Journal of Basic and Applied Sciences* **10**(1), 19 (2021).
13 doi:10.1186/s43088-021-00109-8
- 14 26. Zahm, S., Bonde, J.P., Chiu, W.A., Hoppin, J., Kanno, J., Abdallah, M., Blystone, C.R.,
15 Calkins, M.M., Dong, G.-H., Dorman, D.C., Fry, R., Guo, H., Haug, L.S., Hofmann,
16 J.N., Iwasaki, M., Machala, M., Mancini, F.R., Maria-Engler, S.S., Møller, P., Ng, J.C.,
17 Pallardy, M., Post, G.B., Salihovic, S., Schlezinger, J., Soshilov, A., Steenland, K.,
18 Steffensen, I.-L., Tryndyak, V., White, A., Woskie, S., Fletcher, T., Ahmadi, A.,
19 Ahmadi, N., Benbrahim-Tallaa, L., Bijoux, W., Chittiboyina, S., de Conti, A., Facchin,
20 C., Madia, F., Mattock, H., Merdas, M., Pasqual, E., Suonio, E., Viegas, S., Zupunski,
21 L., Wedekind, R., Schubauer-Berigan, M.K.: Carcinogenicity of perfluorooctanoic
22 acid and perfluorooctanesulfonic acid. *The Lancet Oncology* **In Press, Corrected**
23 **Proof** (2023). doi:10.1016/S1470-2045(23)00622-8
- 24 27. UE Water Directive: Directive (EU) 2020/2184 of the European Parliament and of the
25 Council of 16 December 2020 on the quality of water intended for human
26 consumption (recast) (Text with EEA relevance). *Official Journal of the European*
27 *Union* **63**(2), 1–63 (2020). doi:<http://data.europa.eu/eli/dir/2020/2184/oj>
- 28 28. Dong, H., Xu, L., Mao, Y., Wang, Y., Duan, S., Lian, J., Li, J., Yu, J., Qiang, Z.: Effective
29 abatement of 29 pesticides in full-scale advanced treatment processes of drinking
30 water: From concentration to human exposure risk. *J Hazard Mater* **403**, 123986
31 (2021). doi:<https://doi.org/10.1016/j.jhazmat.2020.123986>
- 32 29. El-Nahhal, I., El-Nahhal, Y.: Pesticide residues in drinking water, their potential risk to
33 human health and removal options. *J Environ Manage* **299**, 113611 (2021).
34 doi:<https://doi.org/10.1016/j.jenvman.2021.113611>
- 35 30. Domergue, L., Cimetière, N., Giraudet, S., Cloirec, P.L.: Adsorption onto granular
36 activated carbons of a mixture of pesticides and their metabolites at trace
37 concentrations in groundwater. *J Environ Chem Eng* **10**(5), 108218 (2022).
38 doi:<https://doi.org/10.1016/j.jece.2022.108218>
- 39 31. Menya, E., Jjagwe, J., Kalibbala, H.M., Storz, H., Olupot, P.W.: Progress in deployment of
40 biomass-based activated carbon in point-of-use filters for removal of emerging
41 contaminants from water: A review. *Chemical Engineering Research and Design* **192**,
42 412–440 (2023). doi:<https://doi.org/10.1016/j.cherd.2023.02.045>
- 43 32. Viegas, R.M.C., Mestre, A.S., Mesquita, E., Machuqueiro, M., Andrade, M.A., Carvalho,
44 A.P., Rosa, M.J.: Key Factors for Activated Carbon Adsorption of Pharmaceutical
45 Compounds from Wastewaters: A Multivariate Modelling Approach. *Water* **14**(2)
46 (2022). doi:10.3390/w14020166
- 47 33. Sellaoui, L., Abdulaziz, F., Chebaane, S., Manai, L., Azhary, A., Alsehli, A.H.,
48 Alsowaygh, M.M., Piscitelli, A., Erto, A.: Adsorption of pharmaceutical pollutants on
49 activated carbon: Physicochemical assessment of the adsorption mechanism via

- 1 advanced modelling. *J Mol Liq* **389**, 122929 (2023).
2 doi:<https://doi.org/10.1016/j.molliq.2023.122929>
- 3 34. Sharma, N., Kumar, V., Sugumar, V., Umesh, M., Sondhi, S., Chakraborty, P., Kaur, K.,
4 Thomas, J., Kamaraj, C., Maitra, S.S.: A comprehensive review on the need for
5 integrated strategies and process modifications for per- and polyfluoroalkyl substances
6 (PFAS) removal: Current insights and future prospects. *Case Studies in Chemical and*
7 *Environmental Engineering* **9**, 100623 (2024).
8 doi:<https://doi.org/10.1016/j.cscee.2024.100623>
- 9 35. Mustafa, M., Kozyatnyk, I., Gallampo, C., Oesterle, P., Östman, M., Tysklind, M.:
10 Regeneration of saturated activated carbon by electro-peroxone and ozonation: Fate of
11 micropollutants and their transformation products. *Sci Tot Environ* **776**, 145723
12 (2021). doi:<https://doi.org/10.1016/j.scitotenv.2021.145723>
- 13 36. Sonmez Baghirzade, B., Zhang, Y., Reuther, J.F., Saleh, N.B., Venkatesan, A.K., Apul,
14 O.G.: Thermal Regeneration of Spent Granular Activated Carbon Presents an
15 Opportunity to Break the Forever PFAS Cycle. *Environmental Science & Technology*
16 **55**(9), 5608-5619 (2021). doi:10.1021/acs.est.0c08224
- 17 37. Fagbohun, E.O., Wang, Q., Spessato, L., Zheng, Y., Li, W., Olatoye, A.G., Cui, Y.:
18 Physicochemical regeneration of industrial spent activated carbons using a green
19 activating agent and their adsorption for methyl orange. *Surfaces and Interfaces* **29**,
20 101696 (2022). doi:<https://doi.org/10.1016/j.surfin.2021.101696>
- 21 38. Santos, D.H.S., Santos, J.P.T.S., Duarte, J.L.S., Oliveira, L.M.T.M., Tonholo, J., Meili, L.,
22 Zanta, C.L.P.S.: Regeneration of activated carbon adsorbent by anodic and cathodic
23 electrochemical process. *Process Saf Environ Prot* **159**, 1150-1163 (2022).
24 doi:<https://doi.org/10.1016/j.psep.2022.01.083>
- 25 39. Yang, Y., Zhong, Z., Li, J., Du, H., Li, Z.: Efficient with low-cost removal and adsorption
26 mechanisms of norfloxacin, ciprofloxacin and ofloxacin on modified thermal kaolin:
27 experimental and theoretical studies. *J Hazard Mater* **430**, 128500 (2022).
28 doi:<https://doi.org/10.1016/j.jhazmat.2022.128500>
- 29 40. Suárez, L., Benavente-Ferraces, I., Plaza, C., de Pascual-Teresa, S., Suárez-Ruiz, I.,
30 Centeno, T.A.: Hydrothermal carbonization as a sustainable strategy for integral
31 valorisation of apple waste. *Bioresour Technol.* **309**, 123395 (2020).
32 doi:<https://doi.org/10.1016/j.biortech.2020.123395>
- 33 41. Jjagwe, J., Olupot, P.W., Menya, E., Kalibbala, H.M.: Synthesis and Application of
34 Granular Activated Carbon from Biomass Waste Materials for Water Treatment: A
35 Review. *Journal of Bioresources and Bioproducts* **6**(4), 292-322 (2021).
36 doi:<https://doi.org/10.1016/j.jobab.2021.03.003>
- 37 42. Lewoyehu, M.: Comprehensive review on synthesis and application of activated carbon
38 from agricultural residues for the remediation of venomous pollutants in wastewater. *J*
39 *Anal Appl Pyrol.* **159**, 105279 (2021). doi:<https://doi.org/10.1016/j.jaap.2021.105279>
- 40 43. Lobato-Peralta, D.R., Duque-Brito, E., Ayala-Cortés, A., Arias, D.M., Longoria, A.,
41 Cuentas-Gallegos, A.K., Sebastian, P.J., Okoye, P.U.: Advances in activated carbon
42 modification, surface heteroatom configuration, reactor strategies, and regeneration
43 methods for enhanced wastewater treatment. *J Environ Chem Eng* **9**(4), 105626
44 (2021). doi:<https://doi.org/10.1016/j.jece.2021.105626>
- 45 44. Melliti, A., Touihri, M., Kofroňová, J., Hannachi, C., Sellaoui, L., Bonilla-Petriciolet, A.,
46 Vurm, R.: Sustainable removal of caffeine and acetaminophen from water using
47 biomass waste-derived activated carbon: Synthesis, characterization, and modelling.
48 *Chemosphere* **355**, 141787 (2024).
49 doi:<https://doi.org/10.1016/j.chemosphere.2024.141787>

- 1 45. Marrakchi, F., Ahmed, M.J., Khanday, W.A., Asif, M., Hameed, B.H.: Mesoporous-
2 activated carbon prepared from chitosan flakes via single-step sodium hydroxide
3 activation for the adsorption of methylene blue. *International Journal of Biological*
4 *Macromolecules* **98**, 233-239 (2017).
5 doi:<https://doi.org/10.1016/j.ijbiomac.2017.01.119>
- 6 46. Khanday, W.A., Marrakchi, F., Asif, M., Hameed, B.H.: Mesoporous zeolite-activated
7 carbon composite from oil palm ash as an effective adsorbent for methylene blue. *J*
8 *Taiwan Inst Chem Eng* **70**, 32-41 (2017).
9 doi:<https://doi.org/10.1016/j.jtice.2016.10.029>
- 10 47. Islam, M.A., Ahmed, M.J., Khanday, W.A., Asif, M., Hameed, B.H.: Mesoporous
11 activated carbon prepared from NaOH activation of rattan (*Lacosperma*
12 *secundiflorum*) hydrochar for methylene blue removal. *Ecotoxicology and*
13 *Environmental Safety* **138**, 279-285 (2017).
14 doi:<https://doi.org/10.1016/j.ecoenv.2017.01.010>
- 15 48. Islam, M.A., Sabar, S., Benhouria, A., Khanday, W.A., Asif, M., Hameed, B.H.:
16 Nanoporous activated carbon prepared from karanj (*Pongamia pinnata*) fruit hulls for
17 methylene blue adsorption. *J Taiwan Inst Chem Eng* **74**, 96-104 (2017).
18 doi:<https://doi.org/10.1016/j.jtice.2017.01.016>
- 19 49. Khanday, W.A., Ahmed, M.J., Okoye, P.U., Hummadi, E.H., Hameed, B.H.: Single-step
20 pyrolysis of phosphoric acid-activated chitin for efficient adsorption of cephalixin
21 antibiotic. *Bioresource Technol.* **280**, 255-259 (2019).
22 doi:<https://doi.org/10.1016/j.biortech.2019.02.003>
- 23 50. Marrakchi, F., Khanday, W.A., Asif, M., Hameed, B.H.: Cross-linked chitosan/sepiolite
24 composite for the adsorption of methylene blue and reactive orange 16. *International*
25 *Journal of Biological Macromolecules* **93**, 1231-1239 (2016).
26 doi:<https://doi.org/10.1016/j.ijbiomac.2016.09.069>
- 27 51. Khanday, W.A., Asif, M., Hameed, B.H.: Cross-linked beads of activated oil palm ash
28 zeolite/chitosan composite as a bio-adsorbent for the removal of methylene blue and
29 acid blue 29 dyes. *International Journal of Biological Macromolecules* **95**, 895-902
30 (2017). doi:<https://doi.org/10.1016/j.ijbiomac.2016.10.075>
- 31 52. Khanday, W.A., Hameed, B.H.: Zeolite-hydroxyapatite-activated oil palm ash composite
32 for antibiotic tetracycline adsorption. *Fuel* **215**, 499-505 (2018).
33 doi:<https://doi.org/10.1016/j.fuel.2017.11.068>
- 34 53. Ramos, P., Singh Kalra, S., Johnson, N.W., Khor, C.M., Borthakur, A., Cranmer, B.,
35 Dooley, G., Mohanty, S.K., Jassby, D., Blotvogel, J., Mahendra, S.: Enhanced
36 removal of per- and polyfluoroalkyl substances in complex matrices by
37 polyDADMAC-coated regenerable granular activated carbon. *Environ Pollu* **294**,
38 118603 (2022). doi:<https://doi.org/10.1016/j.envpol.2021.118603>
- 39 54. Mudhoo, A., Gautam, R.K., Ncibi, M.C., Zhao, F., Garg, V.K., Sillanpää, M.: Green
40 synthesis, activation and functionalization of adsorbents for dye sequestration.
41 *Environmental Chemistry Letters* **17**(1), 157-193 (2019). doi:10.1007/s10311-018-
42 0784-x
- 43 55. Dou, W., Wang, J., Yao, Z., Xiao, W., Huang, M., Zhang, L.: A critical review of
44 hemoperfusion adsorbents: materials, functionalization and matrix structure selection.
45 *Materials Advances* **3**(2), 918-930 (2022). doi:10.1039/D1MA00892G
- 46 56. Duarte, E.D.V., Oliveira, M.G., Spaoloni, M.P., Costa, H.P.S., Silva, T.L.d., Silva,
47 M.G.C.d., Vieira, M.G.A.: Adsorption of pharmaceutical products from aqueous
48 solutions on functionalized carbon nanotubes by conventional and green methods: A
49 critical review. *J Clean Prod* **372**, 133743 (2022).
50 doi:<https://doi.org/10.1016/j.jclepro.2022.133743>

- 1 57. Kang, J.-K., Kim, M.-G., Kim, S.-B., Jeong, S., Oh, J.-E.: Comparative study on
2 Perfluoro(2-methyl-3-oxahexanoic) acid removal by quaternary ammonium
3 functionalized silica gel and granular activated carbon from batch and column
4 experiments and molecular simulation-based interpretation. *Sci Tot Environ* **926**,
5 171753 (2024). doi:<https://doi.org/10.1016/j.scitotenv.2024.171753>
- 6 58. Kasula, M., Pala, J., Esfahani, M.R.: Designing Super Fine Activated Carbon-
7 Functionalized Thin-Film Nanocomposite Membranes for Adsorptive Removal of Per-
8 and Poly-Fluoroalkyl Substances. *ACS Applied Engineering Materials* **2**(1), 143-155
9 (2024). doi:10.1021/acsaenm.3c00670
- 10 59. Garba, Z.N., Zhou, W., Lawan, I., Zhang, M., Yuan, Z.: Enhanced removal of prometryn
11 using copper modified microcrystalline cellulose (Cu-MCC): optimization, isotherm,
12 kinetics and regeneration studies. *Cellulose* **26**(10), 6241-6258 (2019).
13 doi:10.1007/s10570-019-02531-9
- 14 60. Brunauer, S., Emmet, P.H., Teller, E.: Adsorption of gases in multimolecular layers. *J*
15 *American Chem Society*(60), 309–319 (1938). doi:10.1021/ja01269a023
- 16 61. Jagiello, J., Olivier, J.P.: 2D-NLDFT adsorption models for carbon slit-shaped pores with
17 surface energetical heterogeneity and geometrical corrugation. *Carbon* **55**, 70-80
18 (2013). doi:10.1016/j.carbon.2012.12.011
- 19 62. Jagiello, J., Ania, C., Parra, J.B., Cook, C.: Dual gas analysis of microporous carbons
20 using 2D-NLDFT heterogeneous surface model and combined adsorption data of N₂
21 and CO₂. *Carbon* **91**, 330-337 (2015). doi:10.1016/j.carbon.2015.05.004
- 22 63. Jagiello, J., Jaroniec, M.: 2D-NLDFT adsorption models for porous oxides with
23 corrugated cylindrical pores. *J Colloid Interface Sci* **532**, 588-597 (2018).
24 doi:<https://doi.org/10.1016/j.jcis.2018.08.021>
- 25 64. Jagiello, J., Kenvin, J., Celzard, A., Fierro, V.: Enhanced resolution of ultra micropore size
26 determination of biochars and activated carbons by dual gas analysis using N₂ and
27 CO₂ with 2D-NLDFT adsorption models. *Carbon* **144**, 206-215 (2019).
28 doi:<https://doi.org/10.1016/j.carbon.2018.12.028>
- 29 65. Mbarki, F., Selmi, T., Kesraoui, A., Seffen, M.: Low-cost activated carbon preparation
30 from Corn stigmata fibers chemically activated using H₃PO₄, ZnCl₂ and KOH: Study
31 of methylene blue adsorption, stochastic isotherm and fractal kinetic. *Ind Crops Prod*
32 **178**, 114546 (2022). doi:<https://doi.org/10.1016/j.indcrop.2022.114546>
- 33 66. Selmi, T., Sanchez-Sanchez, A., Gadonneix, P., Jagiello, J., Seffen, M., Sammouda, H.,
34 Celzard, A., Fierro, V.: Tetracycline removal with activated carbons produced by
35 hydrothermal carbonisation of Agave americana fibres and mimosa tannin. *Ind Crops*
36 *Prod* **115**, 146-157 (2018). doi:<https://doi.org/10.1016/j.indcrop.2018.02.005>
- 37 67. Nielsen, L., Biggs, M.J., Skinner, W., Bandosz, T.J.: The effects of activated carbon
38 surface features on the reactive adsorption of carbamazepine and sulfamethoxazole.
39 *Carbon* **80**, 419-432 (2014). doi:<https://doi.org/10.1016/j.carbon.2014.08.081>
- 40 68. Seredych, M., Biggs, M.J., Bandosz, T.J.: Oxygen reduction on chemically heterogeneous
41 iron-containing nanoporous carbon: The effects of specific surface functionalities.
42 *Microporous Mesoporous Mater* **221**, 137-149 (2016).
43 doi:<http://doi.org/10.1016/j.micromeso.2015.09.032>
- 44 69. Brita. doi:<https://www.brita.fr/>
- 45 70. Lagergren, S.: Zur Theorie der Sogenannten Adsorption Gelöster Stoffe, *Kungliga*
46 *Svenska Vetenskapsakade- miens. Handlingar* **24**(4), 1-39 (1898).
- 47 71. Ho, Y.S., McKay, G.: Pseudo-second order model for sorption processes. *Process*
48 *Biochem* **34**(5), 451-465 (1999). doi:[http://doi.org/10.1016/S0032-9592\(98\)00112-5](http://doi.org/10.1016/S0032-9592(98)00112-5)
- 49 72. Brouers, F.: The fractal (BSf) kinetics equation and its approximations. *J Mod Phys* **5**(16),
50 1594 (2014). doi:doi.org/10.4236/jmp.2014.516160

- 1 73. Selmi, T., Seffen, M., Sammouda, H., Sandrine, M., Jagiello, J., Celzard, A., Fierro, V.:
2 Physical meaning of the parameters used in fractal kinetic and generalised adsorption
3 models of Brouers–Sotolongo. *Adsorption* **24**(1), 11-27 (2018). doi:10.1007/s10450-
4 017-9927-9
- 5 74. Freundlich, H.: Over the adsorption in solution. *J Phys Chem* **57**, 385-471 (1906).
- 6 75. Langmuir, I.: The adsorption of gases on plane surfaces of glass, mica, and platinum. *J*
7 *American Chem Society* **40**, 1361 (1918).
- 8 76. Brouers, F.: Sorption Isotherms and Probability Theory of Complex Systems.
9 arXiv:1309.5340 (2013).
- 10 77. Brouers, F.: Statistical foundation of empirical isotherms. *Open J Stat* **4**(09), 687-701
11 (2014). doi:<http://dx.doi.org/10.4236/ojs.2014.49064>
- 12 78. Sellaoui, L., Tolga, D., Ali Rıza, K., Salah, K., Abdelmottaleb, B.L.: A new statistical
13 physics model to interpret the binary adsorption isotherms of lead and zinc on
14 activated carbon. *J Mol Liq* (2015). doi:10.1016/j.molliq.2015.12.080
- 15 79. Sellaoui, L., Guedidi, H., Knani, S., Reinert, L., Duclaux, L., Ben Lamine, A.: Application
16 of statistical physics formalism to the modeling of adsorption isotherms of ibuprofen
17 on activated carbon. *Fluid Phase Equilibria* **387**, 103-110 (2015).
18 doi:<https://doi.org/10.1016/j.fluid.2014.12.018>
- 19 80. Yahia, M.B., Gerhardt, R., Sellaoui, L., Al-Zahrani, H.Y.S., Inácio, A.P.O., Dias, D.,
20 Cadaval, T.R.S.A., de Almeida Pinto, L.A., Bonilla-Petriciolet, A., Badawi, M.: An
21 emerging application of chitosan and chitosan/spirulina films for Pb²⁺ adsorption:
22 New physicochemical insights via experimental and theoretical studies. *Separation*
23 *and Purification Technology* **337**, 126451 (2024).
24 doi:<https://doi.org/10.1016/j.seppur.2024.126451>
- 25 81. Sellaoui, L., Dhaouadi, F., Deghrigue, M., Bouzidi, M., Khmissi, H., Dotto, G.L.,
26 Oliveira, M.L.S., Silva, L.F.O., Erto, A., Ernst, B., Badawi, M.: A multilayer
27 adsorption of perfluorohexanesulfonic and perfluorobutanesulfonic acids on bio-based
28 polyurethane/chitosan foam: Advanced interpretation of the adsorption mechanism.
29 *Chem Eng J*, 151173 (2024). doi:<https://doi.org/10.1016/j.cej.2024.151173>
- 30 82. Li, Y., Wang, M., Shan, Y., Liu, J., Han, L., Liu, X.: Adsorption characteristics and
31 molecular mechanisms of ionic organic pollutants on bone char. *J Mol Liq* **400**,
32 124624 (2024). doi:<https://doi.org/10.1016/j.molliq.2024.124624>
- 33 83. Thommes, M., Kaneko, K., Neimark Alexander, V., Olivier James, P., Rodriguez-Reinoso,
34 F., Rouquerol, J., Sing Kenneth, S.W.: Physisorption of gases, with special reference to
35 the evaluation of surface area and pore size distribution (IUPAC Technical Report). In:
36 *Pure and Applied Chemistry*, vol. 87. vol. 9-10, p. 1051. (2015)
- 37 84. Kim, J.G., Bai, B.C.: A Chemical Safety Assessment of Lyocell-Based Activated Carbon
38 Fiber with a High Surface Area through the Evaluation of HCl Gas Adsorption and
39 Electrochemical Properties. *Separations* **11**(3), 79 (2024).
- 40 85. Selmi, T., Enaïme, G., Kesraoui, A., Baçaoui, A., Seffen, M.: Dye removal by activated
41 carbon produced from *Agave americana* fibers: stochastic isotherm and fractal kinetic
42 studies. *Environ Sci Pollut Res* **28**(34), 46580-46591 (2021). doi:10.1007/s11356-020-
43 10768-2
- 44 86. Hayrera, F.O., Kim, D.-G., Ko, S.-O.: Effects of Chemical Activation Conditions on
45 Hierarchical Porous Carbon via Oxytetracycline Adsorption. *Water* **15**(17), 3146
46 (2023).
- 47 87. Kwiatkowski, M., Belver, C., Bedia, J.: Effect of synthesis conditions on the porous
48 texture of activated carbons obtained from Tara Rubber by FeCl₃ activation. *Scientific*
49 *Reports* **14**(1), 2266 (2024). doi:10.1038/s41598-024-52112-5

- 1 88. Al-Musawi, T.J., Brouers, F., Zarrabi, M., Noroozi, R.: What can the use of well-defined
2 statistical functions of pollutants sorption kinetics teach us? A case study of cyanide
3 sorption onto LTA zeolite nanoparticles. *Environmental Technology & Innovation* **10**,
4 46-54 (2018). doi:<https://doi.org/10.1016/j.eti.2018.01.003>
- 5 89. Selmi, T., Seffen, M., Celzard, A., Fierro, V.: Effect of the adsorption pH and temperature
6 on the parameters of the Brouers–Sotolongo models. *Environ Sci Pollut Res* **27**(19),
7 23437-23446 (2020). doi:10.1007/s11356-018-3835-8
- 8 90. Kesraoui, A., Selmi, T., Seffen, M., Brouers, F.: Influence of alternating current on the
9 adsorption of indigo carmine. *Environ Sci Pollut Res* **24**(11), 9940-9950 (2017).
10 doi:10.1007/s11356-016-7201-4
- 11 91. Mbarki, F., Selmi, T., Kesraoui, A., Seffen, M., Gadonneix, P., Celzard, A., Fierro, V.:
12 Hydrothermal pre-treatment, an efficient tool to improve activated carbon
13 performances. *Ind Crops Prod* **140**, 111717 (2019).
14 doi:<https://doi.org/10.1016/j.indcrop.2019.111717>
- 15 92. Selmi, T., Seffen, M., Brouers, F., Fierro, V., Sammouda, H.: Adsorption of Model Dyes
16 Onto Porous Materials: Effect of pH and Temperature on the Parameters of Brouers-
17 Sotolongo Kinetic Fractal and Generalized Isotherm. In: Kallel, A., Ksibi, M., Ben
18 Dhia, H., Khélifi, N. (eds.) *Recent Advances in Environmental Science from the Euro-
19 Mediterranean and Surrounding Regions: Proceedings of Euro-Mediterranean
20 Conference for Environmental Integration (EMCEI-1), Tunisia 2017*. pp. 1039-1041.
21 Springer International Publishing, Cham (2018)
- 22 93. Pereira, D., Gil, M.V., Esteves, V.I., Silva, N.J.O., Otero, M., Calisto, V.: Ex-situ magnetic
23 activated carbon for the adsorption of three pharmaceuticals with distinct
24 physicochemical properties from real wastewater. *J Hazard Mater* **443**, 130258 (2023).
25 doi:<https://doi.org/10.1016/j.jhazmat.2022.130258>
- 26 94. Andrunik, M., Skalny, M., Gajewska, M., Marzec, M., Bajda, T.: Comparison of pesticide
27 adsorption efficiencies of zeolites and zeolite-carbon composites and their
28 regeneration possibilities. *Heliyon* **9**(10) (2023). doi:10.1016/j.heliyon.2023.e20572
- 29 95. Hamid, H., Nicomel, N.R., Mohamed, B.A., Abida, O., Li, L.Y.: Adsorption and leaching
30 of fluorotelomer compounds and perfluoroalkyl acids in aqueous media by activated
31 carbon prepared from municipal biosolids. *J Environ Manage* **358**, 120839 (2024).
32 doi:<https://doi.org/10.1016/j.jenvman.2024.120839>
- 33 96. Vigdorowitsch, M., Pchelintsev, A., Tsygankova, L., Tanygina, E.: Freundlich Isotherm:
34 An Adsorption Model Complete Framework. *Applied Sciences* **11**(17), 8078 (2021).
- 35 97. Brouers, F., Al-Musawi, T.J.: On the optimal use of isotherm models for the
36 characterization of biosorption of lead onto algae. *J Mol Liq* **212**, 46-51 (2015).
37 doi:10.1016/j.molliq.2015.08.054
- 38 98. Atrous, M., Torkia, Y.B., Selmi, T., Bouzid, M., Seffen, M., Lamine, A.B.: Tetracycline
39 Adsorption onto Agave Americana Activated Carbon: Studies of Physicochemical
40 Parameters and Porous Structure. *Theoretical and Experimental Chemistry* (2021).
41 doi:10.1007/s11237-021-09698-y
- 42 99. Gagliano, E., Sgroi, M., Falciglia, P.P., Vagliasindi, F.G.A., Roccaro, P.: Removal of poly-
43 and perfluoroalkyl substances (PFAS) from water by adsorption: Role of PFAS chain
44 length, effect of organic matter and challenges in adsorbent regeneration. *Water Res*
45 **171**, 115381 (2020). doi:<https://doi.org/10.1016/j.watres.2019.115381>
- 46 100. Cai, W., Navarro, D.A., Du, J., Ying, G., Yang, B., McLaughlin, M.J., Kookana, R.S.:
47 Increasing ionic strength and valency of cations enhance sorption through
48 hydrophobic interactions of PFAS with soil surfaces. *Sci Tot Environ* **817**, 152975
49 (2022). doi:<https://doi.org/10.1016/j.scitotenv.2022.152975>

- 1 101. Kabiri, S., Monaghan, C.L., Navarro, D., McLaughlin, M.J.: Hydrophobic interaction is
2 the dominant mechanism of zwitterionic PFAS adsorption to carbon-based sorptive
3 materials in water and soil. *Environmental Science: Water Research & Technology*
4 **10**(2), 420-430 (2024). doi:10.1039/D3EW00550J
- 5 102. Gomis-Berenguer, A., Laidin, I., Renoncial, S., Cagnon, B.: Study of enantioselective
6 metolachlor adsorption by activated carbons. *RSC Adv* **10**(66), 40321-40328 (2020).
7 doi:10.1039/D0RA07745C
- 8 103. Gomis-Berenguer, A., Sidoli, P., Cagnon, B.: Adsorption of Metolachlor and Its
9 Transformation Products, ESA and OXA, on Activated Carbons. *Applied Sciences*
10 **11**(16), 7342 (2021).
- 11 104. Bernal, V., Erto, A., Giraldo, L., Moreno-Piraján, J.C.: Effect of Solution pH on the
12 Adsorption of Paracetamol on Chemically Modified Activated Carbons. *Molecules*
13 **22**(7), 1032 (2017).
- 14 105. Bizi, M., EL Bachra, F.-E.: Transport of Carbamazepine, Ciprofloxacin and
15 Sulfamethoxazole in Activated Carbon: Solubility and Relationships between
16 Structure and Diffusional Parameters. *Molecules* **26**(23), 7318 (2021).
- 17 106. Mestre, A.S., Viegas, R.M.C., Mesquita, E., Rosa, M.J., Carvalho, A.P.: Engineered pine
18 nut shell derived activated carbons for improved removal of recalcitrant
19 pharmaceuticals in urban wastewater treatment. *J Hazard Mater* **437**, 129319 (2022).
20 doi:<https://doi.org/10.1016/j.jhazmat.2022.129319>
- 21 107. PubChem: National Center for Biotechnology Information. PubChem Compound
22 Summary for CID 2256, Atrazine. Retrieved June 1, 2023 from
23 <https://pubchem.ncbi.nlm.nih.gov/compound/Atrazine>. (2023).
- 24 108. Faur, C., Métivier-Pignon, H., Le Cloirec, P.: Multicomponent Adsorption of Pesticides
25 onto Activated Carbon Fibers. *Adsorption* **11**(5), 479-490 (2005). doi:10.1007/s10450-
26 005-5607-2
27
28

1	List of Figures	
2	Figure 1: (A) N ₂ adsorption-desorption isotherms; (B) pore size distributions (PSD); and (C)	
3	cumulative pore volumes of charcoal activated at 850 °C and different activation times. (D)	
4	Variation of BET area as function of burn-off after activation at 850 and 900 °C.	14
5	Figure 2: (A) N ₂ adsorption-desorption isotherm and (B) micro and mesopore volumes for	
6	AC850°C-2h compared with Brita AC and F300 commercial activated carbons.....	16
7	Figure 3: Distribution of surface functional groups as a function of pKa for the three ACs	
8	under study.	18
9	Figure 4: Adsorption kinetic studies of micropollutants: (A) pesticides; (B) pharmaceuticals;	
10	and (C) PFAS on AC850°C-2h, and associated non-linear fits using PSO, PSO and BSf	
11	models.	23
12	Figure 5: Non-linear fits of the adsorption isotherms of micropollutants studied on	
13	AC850°C2h using various models.	26
14	Figure 6: Possible micropollutant adsorption mechanisms on activated carbon.	31
15	Figure 7: ATZ removal by AC850°C-2h compared with Brita AC and F300 commercial ACs	
16	at different contact times and initial concentrations: (A) C _i = 1 mg/L; (B) = C _i = 5 mg/L; and	
17	(C) C _i = 10 mg/L.	34
18		
19		
20		

1 **List of Tables**

2 Table 1: Different parameters used for adsorption tests..... 8

3 Table 2: Interaction scenarios between molecules and active sites as function of n 28

4